

Periodic Korteweg-de Vries soliton potentials generate magnetic field strength with excellent quasisymmetry

W. Sengupta,^{1,*} N. Nikulsin,¹ S. Buller,¹ R. Madan,^{1,2} E.J. Paul,³
R. Nies,^{1,2} A.A. Kaptanoglu,⁴ S.R. Hudson,² and A. Bhattacharjee¹

¹*Department of Astrophysical Sciences, Princeton University, Princeton, NJ, 08543*

²*Princeton Plasma Physics Laboratory, Princeton, NJ, 08540*

³*Columbia University, New York, NY 10027, USA*

⁴*Courant Institute of Mathematical Sciences, New York University, New York, NY 10012, USA*

(Dated: May 27, 2024)

Quasisymmetry (QS) is a hidden symmetry of the magnetic field strength, $|\mathbf{B}|$, that confines charged particles effectively in a three-dimensional toroidal plasma equilibrium. Here, we show that QS has a deep connection to the underlying symmetry that makes solitons possible. Our approach uncovers a hidden lower dimensionality of $|\mathbf{B}|$ on a magnetic flux surface, which could make stellarator optimization schemes significantly more efficient. Recent numerical breakthroughs (M. Landreman and E. Paul, *Phys. Rev. Lett.* **128**, 035001 (2022)) have yielded configurations with excellent volumetric QS and surprisingly low magnetic shear. Our approach elucidates why the magnetic shear is low in these configurations. Furthermore, we deduce an upper bound on the maximum toroidal volume that can be quasisymmetric and verify it for the Landreman-Paul precise quasisymmetric (QA) stellarator configuration. In the neighborhood of the outermost surface, we show that the $|\mathbf{B}|$ approaches the form of the 1-soliton reflectionless potential (I. Gjaja and A. Bhattacharjee, *Phys. Rev. Lett.* **68**, 2413 (1992)). We present three independent approaches to demonstrate that quasisymmetric $|\mathbf{B}|$ is described by well-known integrable systems such as the Korteweg-de Vries (KdV) equation. The first approach is weakly nonlinear multiscale perturbation theory, which highlights the crucial role that magnetic shear plays in QS. We show that the overdetermined problem of finding quasisymmetric vacuum fields admits solutions for which the rotational transform is not free but highly constrained. We obtain the KdV equation (and, more specifically, Gardner's equation for certain choices of parameters). Our second approach is non-perturbative and based on ensuring single-valuedness of $|\mathbf{B}|$, which directly leads to its Painlevé property shared by the KdV equation. Our third approach uses machine learning, trained on a large dataset of numerically optimized quasisymmetric stellarators. We robustly recover the KdV (and Gardner's) equation from the data.

I. INTRODUCTION

Physical systems possessing a hidden symmetry attract serious attention [1–6] because of the far-reaching impact of the symmetry on the physical properties of the systems. The hidden symmetry manifests only in special coordinates, which are constructed, along with the invariants, as part of the solution to the problem. In the presence of hidden symmetries, the partial differential equations (PDEs) governing classical dynamical fields often reduce to integrable PDEs [5–7]. An example of the latter is the well-known Korteweg-de Vries (KdV) equation with soliton solutions [8, 9].

In plasma physics, a hidden symmetry called *quasisymmetry* (QS)[10, 11], forces the magnetic field strength, $B = |\mathbf{B}|$, to be symmetric [10, 12], whereas \mathbf{B} itself depends on all three spatial coordinates, and is thus said to be three-dimensional (3D). The similarity of this symmetry with particle relabelling symmetries [13, 14] is known

[12, 15] but yet to be fully explored. The hidden symmetry in B makes the bounce action (second adiabatic invariant), J_{\parallel} , independent of the field-line label [11], which guarantees excellent particle confinement on a torus. The three-dimensional nature of \mathbf{B} allows stellarators to avoid intrinsic difficulties (such as powerful transients) associated with large plasma currents in axisymmetric configurations.

It is currently unknown whether QS can be achieved exactly in a toroidal volume for a magnetic field that satisfies the constraint of force balance in ideal magnetohydrodynamics (MHD) [16]. The problem is of fundamental importance and potentially significant for the design of next-generation stellarator fusion reactors. Analytical results [17–20] seem to indicate that in the presence of scalar plasma pressure, the resulting 3D nonlinear system of PDEs does not have solutions in a toroidal volume [17, 18, 20–23]. In particular, the near-axis expansion (NAE), which is an asymptotic expansion in the distance from the magnetic axis [24–26], when applied to QS [17, 18, 27], becomes overdetermined beyond the second-order. Moreover, NAEs are typically divergent beyond second-order (L. Fu, private communica-

* Email: wsengupta@princeton.edu

tion). Overdetermined problems do not generally have solutions. Even when they have solutions, they can be subject to restrictive constraints. For example, in the particular case of isodynamic magnetic fields, which satisfy a constraint more restrictive than QS [11, 28], it has been shown [28, 29] that if a solution exists, it must be essentially 2D: either axisymmetric like a tokamak or a helically symmetric straight stellarator.

On the other hand, numerical 3D solutions with a precise level of QS and MHD force balance have been obtained through large-scale numerical optimization, hinting at the possible existence of special and physically interesting toroidal stellarator solutions to the overdetermined problem. However, the numerical search over a typically vast parameter space obscures insight into the quasisymmetric stellarator configuration space that permits precise solutions.

In this work, we demonstrate that QS admits a class of analytic B that is a periodic solution [9, 30] of the KdV equation. We proceed along three independent lines of inquiry to support our result. In the first approach, we formulate the overdetermined problem of QS in a vacuum field in close analogy with the equations that arise in the theory of shallow water waves. Analogously to the water wave theory, we highlight the importance of a traveling wave (TW) frame and the existence of longer length scales in QS. Using a weakly nonlinear multiscale approach, we show that under some assumptions, the magnetic field strength must satisfy the KdV equation whose solutions satisfy the overdetermined set of equations perturbatively. We can also show that for small rotational transform, the next order corrections that are needed will lead to Gardner's equation, a generalization of the KdV equation [31–33]. As in the isodynamic case [28], we show that the rotational transform is not free but highly constrained, and that for a given rotational transform, a perturbative solution of the overdetermination problem of quasisymmetric vacuum fields can be constructed only for some values of the shear. Although the perturbative approach is necessarily approximate, it provides information not only on quasisymmetric B but also the full \mathbf{B} over the entire plasma volume.

In the second approach, starting from the basic definitions and properties of QS, and requiring only analyticity and single-valuedness of B , we show non-perturbatively the connection to the theory of periodic KdV solitons. This approach is complementary to the first approach and is formally exact. In making the connection to soliton theory, we demonstrate how the field-line label independence of the second adiabatic invariant J_{\parallel} and other integrals of B in QS are directly related to the infinite hierarchy of conserved quantities of the KdV equation. The exact analytic solution for B is valid in the entire toroidal volume and reduces to the NAE predictions close to the axis.

Our third approach is data-driven. We use PySINDy[34, 35] to look for relations between B and its

derivatives in the large family of quasi-axisymmetric configurations generated in [36] and the QUASR database [37]. PySINDy employs sparse regression techniques and algorithms to discover governing dynamical systems models from noisy and limited data. We show that over a wide range of configurations and parameters, the KdV equation with the traveling wave form for B holds. As described later in the paper, the only exceptions we found are covered by Gardner's equation.

The connection with periodic KdV solitons allows us to describe B on a magnetic flux surface with only three functions of the magnetic flux, related to the so-called *spectral parameters* [9] of the KdV equation. We show that these functions are closely related to the spectrum of B in Boozer coordinates [11] where the hidden symmetry is manifest, thereby highlighting the low dimensionality of the Boozer spectrum. Furthermore, our analysis shows that the periodicity of B is maintained only when these functions are distinct. Consequently, we can estimate the region of validity of volumetric QS based on where the two spectral parameters intersect (discussed below). Remarkably, near the point of intersection, the connection length (period of B) begins to diverge, and B approaches the form of a reflectionless potential (a single soliton that decays at infinity) [38, 39]. We demonstrate using both data-driven and traditional numerical methods that our analytic theory can describe well the properties of the field strength on a flux surface of the vacuum equilibrium with precise quasi-axisymmetry (QA)[4] and many other optimized quasisymmetric configurations.

II. BASIC FORMULATION OF QUASISYMMETRY

We begin by reviewing some of the known basic properties of QS. Several equivalent [11, 12, 16, 22, 40] mathematical descriptions of QS exist. In this Section, we will briefly discuss the most relevant equations and coordinates to describe QS and point out their inter-relationships.

It can be shown that QS implies the existence of a divergence-free vector field \mathbf{u} that satisfies the overdetermined system [22]

$$\nabla \cdot \mathbf{u} = 0, \quad (1a)$$

$$\mathbf{u} \cdot \nabla B = 0, \quad (1b)$$

$$\mathbf{B} \times \mathbf{u} = \nabla \psi. \quad (1c)$$

It follows directly from (1c) and the divergence-free nature of \mathbf{u} , \mathbf{B} that $\mathbf{u} \cdot \nabla$ and $\mathbf{B} \cdot \nabla$ commute, i.e.,

$$[\mathbf{u} \cdot \nabla, \mathbf{B} \cdot \nabla] = 0. \quad (2)$$

Here, we have used the usual definition of the commutator $[A_1, A_2] \equiv A_1 A_2 - A_2 A_1$ for two operators A_1, A_2 .

The mathematical structure of (1) strongly suggests that \mathbf{u} can be associated with a particle relabelling symmetry group ([13, 14, 41–44] and references therein) with density replaced by the field strength [12, 15]. Therefore, understanding the hidden symmetry behind QS might also be beneficial in understanding Casimirs [13, 45] in fluid dynamics and ideal MHD.

From equation (1c) we can show that

$$\mathbf{u} = (\mathbf{B} \times \nabla\psi - F(\psi)\mathbf{B})/B^2. \quad (3)$$

The condition (1b) then implies

$$\mathbf{B} \times \nabla\psi \cdot \nabla B = F(\psi)\mathbf{B} \cdot \nabla B, \quad (4)$$

which is sometimes called the two-term form [22].

For a vacuum field $\mathbf{B} = G_0\nabla\Phi$ [11, 46],

$$F(\psi) = G_0q_N, \quad q_N \equiv (\iota - N)^{-1}, \quad (5)$$

where ι is the rotational transform, N is the helicity of QS, $2\pi G_0/\mu_0$ is the poloidal current outside the surface and Φ is a toroidal angle. Moreover, the two-term form of QS (equivalently $\mathbf{u} \cdot \nabla B = 0$) for vacuum fields leads to a TW solution for B [47] of the form

$$|\mathbf{B}| = B(\Phi + (F(\psi)/G_0)\alpha, \psi), \quad F(\psi)/G_0 = q_N. \quad (6)$$

Thus, the rotational transform and, hence, the magnetic shear enters the definition of QS (4) in a fundamental way. Furthermore, the TW form of B indicates that in the Boozer coordinate system $(\psi, \vartheta_B, \phi_B)$,

$$\phi_B = \Phi, \quad \vartheta_B = \alpha + (\iota - N)\Phi, \quad |\mathbf{B}| = B(\vartheta_B, \psi), \quad (7)$$

i.e., the field strength B depends only on a single angle ϑ_B . Thus, QS manifests itself in these coordinates. This is true not just for the vacuum field but also in the presence of currents and finite pressure in the plasma.

Another form of QS is the so-called ‘‘triple-product’’ form [12, 22]

$$\nabla\psi \times \nabla B \cdot \nabla (\mathbf{B} \cdot \nabla B) = 0. \quad (8)$$

The two-term and the triple-product form of QS are equivalent under the assumption of irrational ι and continuity on rational surfaces [11]. Alternatively, the form

$$\mathbf{u} = (\nabla\psi \times \nabla B)/\mathbf{B} \cdot \nabla B, \quad (9)$$

is consistent with (3), satisfies (1b), (1c), while (1a) implies (8).

It is useful to use the standard Clebsch coordinate system [11, 48], (ψ, α, ℓ) , such that $\mathbf{B} = \nabla\psi \times \nabla\alpha$ with flux label ψ , field-line label α , and ℓ , the arclength along the magnetic field. We impose suitable toroidal cuts since α is a multi-valued function. The triple-product form (8) now reads [16]

$$\frac{\partial B}{\partial \ell} = f(B, \psi). \quad (10)$$

where f must be a function of ψ and B .

In toroidal geometry, B is subject to the following periodic boundary condition [11]:

$$B(\psi, \alpha, \ell) = B(\psi, \alpha, \ell + L(\psi)). \quad (11)$$

The period of B , $L(\psi)$, is called the connection length and is a quantity of great physical interest [49].

As shown in Appendix A, in (ψ, α, ℓ) coordinates, the $\mathbf{u} \cdot \nabla B = 0$ condition takes the form [16]

$$\partial_\alpha B + H(\psi, \alpha)\partial_\ell B = 0, \quad (12)$$

where $H(\psi, \alpha)$ is independent of ℓ and depends on the definition of the origin of ℓ . It follows from (12) that

$$H(\psi, \alpha) = -\frac{\partial_\alpha B|_\ell}{\partial_\ell B|_\alpha} = \left. \left(\frac{\partial \ell}{\partial \alpha} \right) \right|_B \quad (13)$$

We note that there is a degree of freedom in choosing the (ℓ, α) pair. By transforming to the coordinates $(\bar{\ell}, \alpha)$, where

$$\bar{\ell} \equiv \ell - \int H(\psi, \alpha)d\alpha, \quad (14)$$

we find that

$$\mathbf{u} \cdot \nabla = -\partial_\alpha|_{\bar{\ell}}, \quad \mathbf{B} \cdot \nabla = B\partial_{\bar{\ell}}, \quad (15)$$

The condition (12) then reduces to

$$\partial_\alpha|_{\bar{\ell}} B = 0 \quad \text{i.e.} \quad B = B(\bar{\ell}, \psi). \quad (16)$$

Thus, there exists a special TW frame $(\bar{\ell}, \alpha)$ in QS where the field strength B is independent of α [16]. We show the equivalence of the two TW forms of B given by (7) and (16) in Appendix B 1.

There are, in addition, important integral constraints that follow from the requirements of QS. From the $\partial_\ell B$ condition (10), any integral along the magnetic field line between two points of equal values of $B = B_b$ satisfies

$$\partial_\alpha \int_{B \leq B_b} d\ell F(B; \psi) = 0. \quad (17)$$

The field line independence of the second adiabatic invariant J_\parallel

$$J_\parallel = \oint \sqrt{\mathcal{E} - B} d\ell, \quad (18)$$

where \mathcal{E} is related to the particle energy, is a special case of (17). As a direct consequence of (17), it follows that quasisymmetric B can not have local maxima or minima on a flux surface [11, 50].

The distinctions between the cases of exact symmetry (axisymmetry or helical symmetry), quasisymmetry and omnigenity must now be made clear. For the special cases of exact symmetry, the corresponding symmetry

vectors are the well-known Killing vectors of Euclidean space [40], which implies that \mathbf{u} and \mathbf{B} are completely decoupled, and the symmetric form of \mathbf{B} is determined by \mathbf{u} . Therefore, the condition (1b) can be trivially satisfied. Here, we will focus on the case of 3D QS where \mathbf{u} cannot be posited *a priori*. Consequently, the condition (1b) will impose a nontrivial constraint. In particular, unlike the case of exact symmetry, the functional form of $f(B, \psi)$ in the $\partial_\ell B$ equation will be constrained. We address this question directly in this work.

QS being a special case of omnigenity [11], the integral property (17) also holds for omnigenous magnetic fields. However, significant differences arise because omnigenity is not a local property, and a symmetry vector \mathbf{u} does not exist for omnigenous magnetic fields. Thus, the local conditions such as (4) or (10), which follow from the properties of \mathbf{u} do not hold for omnigenity. It follows that omnigenous fields need not be of the TW form (6). Furthermore, unlike QS [17, 27], omnigenous B cannot be uniformly analytic on a flux surface [51–53].

As a final step, one must impose a force-balance condition. Without imposing force balance, one can exactly satisfy the QS condition order by order in the NAE [23]. However, the nonlinear overdetermination problem that results when the force-balance condition is imposed is severely restrictive [17, 18]. In the next Section, we address this problem head-on by looking at quasisymmetric vacuum fields. To make the problem analytically tractable, we first consider slab geometry (or a flat torus). We then show that the analysis for the general geometry can be carried out in close analogy with the slab geometry under certain additional assumptions.

III. PERTURBATIVE SOLUTION TO THE OVERDETERMINATION PROBLEM OF QS IN VACUUM MAGNETIC FIELDS

With the basic formulation of QS in place, we now take a perturbative approach to solving the overdetermined problem in a quasisymmetric vacuum magnetic field and understand the vital role of magnetic shear in QS. Besides mathematical simplicity, vacuum fields are of great practical relevance since they are usually a point of departure for systematic studies of low plasma-beta systems.

Vacuum fields with a very high degree of QS, obtained through numerical optimization [4], appear to be characterized by exceptionally low magnetic shear. Since magnetic shear plays an essential role in MHD stability theory, it is important to understand if QS is inextricably tied to the low shear of such configurations.

The second-order NAE theory predictions match the precise QS configurations remarkably well [12, 54]. However, the second-order NAE theory cannot readily capture the effects of magnetic shear for quasisymmetric

configurations. The reason behind this is connected to the overdetermination problem. While magnetic shear near the axis needs third and fourth-order contributions [23–25] in the NAE, the quasisymmetric system becomes hopelessly overdetermined beyond second-order.

We will demonstrate here that it is possible to address both the issues of overdetermination and weak magnetic shear. We begin with the observation that the remarkable accuracy with which the flux surface shapes and the magnetic field strength are captured within second-order NAE suggests a multi-scale approach to the QS problem, where the magnetic shear introduces another length scale. Let $\alpha = \theta - \iota(\psi)\phi$ denote the field line label in a straight field line coordinate system (ψ, θ, ϕ) . Its gradient, $\nabla\alpha$, is multi-valued and given by

$$\begin{aligned} \nabla\alpha &= \mathbf{V}_1 + \mathbf{V}_2 \\ \mathbf{V}_1 &\equiv (\nabla\theta - \iota(\psi)\nabla\phi), \quad \mathbf{V}_2 \equiv \iota'(\psi)\phi\nabla\psi \end{aligned} \quad (19)$$

The vector \mathbf{V}_1 is single-valued, whereas \mathbf{V}_2 is not. There are two length scales associated with $\nabla\alpha$

$$L_{\alpha 1}^{-1} \sim |\mathbf{V}_1|, \quad L_{\alpha 2}^{-1} \sim |\mathbf{V}_2| \sim \iota'(\psi)|\nabla\psi|. \quad (20)$$

Near the axis, $|\nabla\theta| \sim \rho^{-1}$, where $\rho = \sqrt{2\psi}$ is the distance from the axis, whereas $|\nabla\phi| \sim R^{-1}$, where R is the typical radius of curvature of the axis and $\rho \ll R$ in the NAE. Thus, the length scale $L_{\alpha 1}^{-1} \sim \rho^{-1}$ near the axis, which represents the typical scale of poloidal variations of surfaces. On the other hand, $L_{\alpha 2}^{-1} \sim \iota'(\psi)|\nabla\psi| \sim \hat{s}\rho$ near the axis, where \hat{s} is the on-axis shear. Thus, $L_{\alpha 2}$ is greater than $L_{\alpha 1}$ by (typically, approximately two) orders of magnitude in the distance from the axis. In particular, for second-order NAE, $L_{\alpha 2}$ tends to infinity since ι is approximated by the on-axis rotational transform ι_0 . As we move further away from the axis, a finite value of $L_{\alpha 2}$ is needed to capture the effect of shear. The two disparate scales $L_{\alpha 1}, L_{\alpha 2}$ clearly provide a basis for a multi-scale approach, akin to the well-known approach in the theory of ballooning modes [55–57].

We propose a free-surface approach to QS with the two scales in mind. We assume that the second-order NAE theory has been used to construct a good volumetric quasisymmetric vacuum field. The NAE solution serves as our inner solution near the axis. The outer free-surface solution arises from the surface expansion approach. Consistent with the observation that NAE predictions for the geometry are surprisingly accurate, we shall assume that the surface expansion can be carried out in a small region around a surface generated using the second-order NAE. The surface expansion allows us to bypass the difficulties of including the effects of shear within the framework of the NAE. The outermost flux surface will be treated as a free surface determined self-consistently by imposing QS and force balance.

An essential step in any multi-scale analysis is to average over the fast scale to obtain an equation that involves only the slow scale. For example, in the study

of ballooning modes near the axis [55], a poloidal averaging of the standard ballooning equation is carried out to average over the fast variation $L_{\alpha 1} \sim \rho$ and obtain a “distilled ballooning equation”, which involves only the longer length scale $L_{\alpha 2} \sim \hat{s}\rho$. A rigorous multiscale NAE program must be carried out for this purpose, which is beyond the scope of the present work. Here, we shall content ourselves with geometries that depend only weakly on the fast scale, thereby bypassing the need for averaging over the fast scale to obtain the “distilled” equations. Vacuum fields in slab and cylindrical geometries offer such possibilities.

In Section III A, we first demonstrate the free-surface approach to solving the overdetermination problem of QS in a vacuum field for slab geometry. The analysis is simplified, and lays bare the balance between dispersion and nonlinearity needed to realize soliton solutions [58]. Once this structure is understood, it essentially carries over with minimal modification to the more general geometry, which we discuss in III B.

A. Vacuum quasisymmetric magnetic field in slab geometry

In this Section, we will demonstrate that the problem of finding quasisymmetric vacuum fields in a slab geometry, utilizing the free-surface approach discussed earlier, can be solved in close analogy with the shallow-water waves under gravity, which also has a free surface. We will show that for small amplitude variations of the free surface, the nonlinearity originating from QS is weak. Magnetic shear plays the analog of gravity in the QS problem, and dispersion comes from higher derivatives due to the surface expansion, with the balance of the weak nonlinearity and the dispersion leading to a KdV equation for B . The functional form of f in the $\partial_\ell B$ in (10) is then shown to be a square root of a cubic polynomial with three real roots. In this way, the cubic polynomial is seen not as a fitting function but one that follows from the construction procedure.

Before we proceed with the calculation, we discuss the assumptions and our strategy. Cartesian coordinates are convenient for the description of the slab geometry. We assume that the inner solution is a vacuum field with straight field lines $\mathbf{B}_0 = B_0 \hat{\mathbf{x}}$ and constant z planes as flux surfaces. We will assume that the rotational transform is close to a low-order rational number. Thus, $q_N = (\iota - N)^{-1}$ will be assumed to be of the form

$$q_N = m/n + \hat{q}, \quad (21)$$

where \hat{q} is a small deviation from the low-order rational. The inner solution is trivially quasisymmetric. We will then carry out a surface expansion around the plane $z = h$ with the outermost free-surface parametrized by $z = h + \eta(x, y)$. The amplitude of $\eta(x, y)$ and h will be

assumed small compared to the characteristic length L along the field line, which allows us to carry out a multiscale analysis for a weakly nonlinear system typical in the theory of shallow-water waves [58]. The justification and the relevance of the assumptions will be made clear in the following.

Exact vacuum fields in slab geometry with closed field lines and nested flux surfaces have been obtained in [59]. As shown in [59], one of the peculiarities of closed field line systems in a slab geometry is that one can always re-orient the coordinate system such that the magnetic field is purely along one of the axes. For a closed field line, tangential to the X, Y plane and $\iota \equiv (\mathbf{B} \cdot \nabla Y) / (\mathbf{B} \cdot \nabla X) = n/m$, this can be achieved through a combination of rotation and dilatation of the coordinates

$$\begin{aligned} z &= m\sqrt{1 + (n/m)^2}Z, \\ x &= m(X + (n/m)Y), \quad y = m(Y - (n/m)X). \end{aligned} \quad (22)$$

It is clear that if the rotational transform is a high-order rational, the mutually prime numbers n, m are large, and the coordinate transform (22) becomes ill-defined owing to the large dilation factor. We also note that if $N = 0$ and $\iota \ll 1$, q_N will be in general large, and a transformation of the form (22) will once again be challenging. Therefore, with the assumption that the rotational transform is nonzero and sufficiently close to a low-order rational, we can assume without loss of generality that the inner solution is given by $\mathbf{B}_0 = B_0 \hat{\mathbf{x}}$.

Let $\mathbf{B} = G_0 \nabla \Phi$ be a vacuum magnetic field with G_0 constant. In the (ψ, α, ℓ) coordinates, the field strength is given by

$$B = G_0 \frac{\partial \Phi}{\partial \ell}. \quad (23)$$

Equivalently, $\Phi_0 = x/L$, where $L \equiv B_0/G_0$. The flux surface and field line labels are given by $\psi_0 = B_0 L z$, $\alpha_0 = -y/L$. Our domain of interest will be the region bounded by $0 \leq x, y \leq L$, $0 \leq \psi \leq \bar{\psi} \equiv B_0 L(h + a)$.

We now develop a weakly nonlinear theory of small but finite amplitude perturbation $\eta(x, y)$ of the surface $z = h$. Since \mathbf{B} is predominantly in the x direction, the flux surfaces, $\psi = \text{const}$, are of the form $z = f(x, y)$. In particular, $z = 0$ and $z = h + \eta(x, y)$ will be chosen to correspond to $\psi = 0$ and $\psi = \bar{\psi}$ respectively. We can then set up the problem as a “free-boundary” problem, where determining the “free-surface” ($\psi = \bar{\psi}$) is itself a part of the solution to the problem.

The basic set of equations for the vacuum quasisymmetric system is

$$\nabla^2 \Phi = 0 \quad (0 \leq z \leq h + \eta) \quad (24a)$$

$$\frac{\partial \Phi}{\partial z} = 0 \quad (z = 0) \quad (24b)$$

$$\frac{\partial \Phi}{\partial \alpha} + H(\psi, \alpha) \frac{\partial \Phi}{\partial \ell} + \hat{q}(\psi) = 0 \quad (z = h + \eta) \quad (24c)$$

$$\nabla \Phi \cdot \nabla \psi = 0 \quad (z = h + \eta) \quad (24d)$$

Equation (24a) is the Laplace equation for Φ , which follows from the current-free and divergence-free nature of the vacuum magnetic field. Note that the Laplace equation holds in the whole domain $0 \leq z \leq h + \eta(x, y)$. The second equation (24b) is the “no-flow” boundary condition on $z = 0$, which denotes the tangency of the magnetic field to the flux surface $z = 0$. The third equation (24c) is the QS condition that follows from $\mathbf{u} \cdot \nabla \Phi = -F(\psi)/G_0$ expressed in (ψ, α, ℓ) coordinates. Here, the function $H(\psi, \alpha)$ is obtained from derivatives of B using (13). (In Appendix B, we show its equivalence to the two-term form (4).) Finally, (24d) is another tangential boundary condition on the flux surface $\psi = \bar{\psi}$. Therefore, equations (24a), (24b), (24d) enforce zero current and existence of flux surfaces at the top and bottom, while (24c) impose QS on the top surface. Although the nestedness of flux surfaces is not guaranteed in generic 3D vacuum fields, we can guarantee nestedness to the lowest nontrivial order in the small amplitude perturbation problem.

The system (24) is mathematically similar to some aspects of the theory of shallow-water waves under gravity. Since our problem has no explicit time, we make α the analog of time. Therefore, in analogy with the shallow-water wave theory [58], we denote the condition (24d) as the “kinematic boundary condition” (KBC), and (24c) as the “generalized Bernoulli” (GB) condition. The differences between water wave theory and QS arise from the difference in the Bernoulli condition and the fact that we treat y (approximately α) as a time-like variable.

In order to proceed systematically with the amplitude expansion, we need to introduce the scales in (x, y, z) and their relation to the various physical quantities. Three length scales are relevant to the problem: L along (x, y) , h along z and a , the amplitude of the perturbation $\eta(x, y)$. With these length scales, we can define two small parameters

$$\epsilon \equiv a/h, \quad \delta \equiv h/L \quad (25)$$

Guided by the “principle of maximal balance” [58, 60], we order

$$\epsilon \sim \delta^2. \quad (26)$$

In the water-wave theory, the relation (26) represents the delicate balance between nonlinearity and dispersion, which is crucial for the existence of solitons. The significance of (26) in the context of vacuum fields can be clarified by NAE theory. The small parameter δ is analogous to the near-axis expansion parameter $\kappa\rho$, which is the product of the axis curvature κ and distance ρ from the axis. The balance (26) then implies that there are second-order corrections to the NAE flux surface shapes due to the magnetic shear. The difference between the actual surface and the second-order NAE predictions being $O(\delta^2)$ is consistent with the results obtained using NAE and standard numerical optimization [12, 54]. We

note that (26) is not the only possible relation for balancing nonlinearity and dispersion [61]. Other possibilities will be discussed in a future publication.

We now proceed with the following normalizations

$$\begin{aligned} x &\rightarrow x/L, \quad y \rightarrow y/L, \quad z \rightarrow z/(\sqrt{\epsilon}L), \quad \ell \rightarrow \ell/L \\ B &\rightarrow B/B_0, \quad \psi \rightarrow \psi/(B_0L^2\sqrt{\epsilon}) \end{aligned} \quad (27)$$

It is convenient to separate the secular part of Φ that leads to the constant magnetic field B_0 such that

$$\Phi = x + \epsilon\varphi, \quad B = 1 + \epsilon\varphi, \ell \quad (28)$$

The small factor ϵ in the second term indicates that we consider only small deviations from the constant B_0 state. The system (24) now reads

$$(\partial_x^2 + \partial_y^2 + \epsilon^{-1}\partial_z^2)\varphi = 0 \quad (0 \leq z \leq 1 + \epsilon\eta) \quad (29a)$$

$$\partial_z\varphi = 0 \quad (z = 0) \quad (29b)$$

$$\epsilon\partial_\alpha\varphi + H(1 + \epsilon\varphi, \ell) + \hat{q} = 0 \quad (z = 1 + \epsilon\eta) \quad (29c)$$

$$\varphi, z = \epsilon\eta, x(1 + \epsilon\varphi, x) + \epsilon^2\varphi, y\eta, y \quad (z = 1 + \epsilon\eta). \quad (29d)$$

We now consider the perturbative solution of the system (29). The details are provided in Appendix B. The solution of (29a) and (29b) is given by

$$\varphi = \left(1 - \epsilon\frac{z^2}{2!}\nabla_\perp^2 + \epsilon^2\frac{z^4}{4!}\nabla_\perp^4 + \dots\right)\mathcal{A}(x, y), \quad (30)$$

where $\nabla_\perp^2 = \partial_x^2 + \partial_y^2$ and $\mathcal{A}(x, y)$ is φ to lowest order, which is yet to be determined.

Next, we note that the field-line following coordinates (ψ, α, ℓ) only appear in the GB condition (29c), obtained above. The separation (28), together with $\partial_z\Phi = O(\epsilon)$, that follows from (30), allows us to conveniently express (ψ, α, ℓ) in terms of the Cartesian (x, y, z) coordinates. Up to $O(\epsilon^2)$, we have

$$\begin{aligned} \ell &= x + O(\epsilon^2) \\ \partial_\ell &= \frac{1}{1 + \frac{\epsilon^2}{2}\varphi, y} (\partial_x + \epsilon\varphi, y\partial_y + \varphi, z\partial_z) \\ \partial_\alpha &= -\frac{\partial_y + \epsilon\eta, y\partial_z}{1 + \epsilon\varphi, x}. \end{aligned} \quad (31)$$

The derivation of these equations is given in Appendix B. With the help of (13), (28) and (31) we can show that

$$\begin{aligned} H &= H_0 + \epsilon H_1 + O(\epsilon^2), \\ H_0 &= \frac{\varphi, xy}{\varphi, xx}, \quad H_1 = \frac{\varphi, y\varphi, yy}{\varphi, xx} - H_0(\varphi, x + 2H_0\varphi, y). \end{aligned} \quad (32)$$

The function \hat{q} , which is assumed to be small, can be expanded as follows:

$$\hat{q} \approx q_0 + \Delta\psi \hat{q}'(\psi) = q_0 + \epsilon\eta q_1, \quad (33)$$

where $\Delta\psi = \epsilon\eta$ is the change in the flux surface. When (32) and (33) are substituted in the GB equation (24c), we obtain

$$\mathcal{A}_{,xy}/\mathcal{A}_{,xx} + q_0 = 0, \quad (34)$$

to lowest order in ϵ . The implication of (34) is that \mathcal{A} is a TW solution of the form

$$\mathcal{A} = \mathcal{A}(\xi, Y), \quad \xi = x - q_0 y, \quad Y = \epsilon y. \quad (35)$$

Here, $Y = \epsilon y$ denotes a longer length scale in y . The TW solution is consistent with (6) expanded to the lowest order in ϵ .

To $O(\epsilon)$, the GB equation (29c) yields

$$-\eta q_1/q_0 = (1 + q_0^2)A_{,\xi} \quad (36)$$

Proceeding with the KBC (29d), we find that the lowest order

$$-\eta = (1 + q_0^2)A_{,\xi}. \quad (37)$$

The consistency of the KBC and the GB equations, or equivalently, the consistency of QS with the force balance, imply

$$q_1 = q_0 + O(\epsilon). \quad (38)$$

To understand the significance of (38) we first note that the magnetic shear is given by

$$\hat{s} \equiv (dq_N/d\psi)/q_N \approx q_1/(m/n + q_0). \quad (39)$$

Thus, (38) implies that the shear is completely determined to $O(\epsilon) \sim O((\kappa\rho)^2)$ by the compatibility of force-balance and QS. The smallness of shear originates from the fact that $q_1 = q_0$ and q_0 is small by construction.

Finally, neglecting quadratic terms in q_0 , the $O(\epsilon)$ KBC leads to the following equation for $\tilde{B} = A_{,\xi}$:

$$2q_0\partial_Y\tilde{B} + 2\tilde{B}\tilde{B}_{,\xi} + \frac{1}{6}\tilde{B}_{,\xi\xi\xi} = 0. \quad (40)$$

Through suitable variable transformations, the above equation can be cast as the standard KdV equation for $B = 1 + \epsilon\tilde{B}$

$$\partial_t B + 6B\partial_x B + \partial_x^3 B = 0. \quad (41)$$

The TW (6) to next order implies that $\partial_Y = c_1\partial_\xi B$, which enables (40) to be integrated twice, resulting in

$$\partial_\ell B = f(B, \psi), \quad f^2 = 2(B_M - B)(B - B_m)(B - B_X). \quad (42)$$

The above form shows that the unknown $f(B, \psi)$ is a square root of a cubic polynomial, with roots B_M, B_m, B_X ; B_M, B_m being the maximum and minimum values of the field strength.

Let us point out some of the important predictions of the slab theory. Firstly, the sum $B_M + B_m + B_X$ is determined by the coefficients of KdV [30], which, as seen from (40) only depends on q_0 . Moreover, as predicted by the NAE theory (Section V) and confirmed numerically (Section VI and Appendix E), the sum of B_M, B_m is essentially a constant equal to the field strength on the axis. Therefore, the third root B_X , must be determined by the ι profile. We shall also numerically verify this observation in Section VI.

Finally, let us discuss the case where q_N can be large or have a steep gradient, which can happen for small ι and $N = 0$. This falls outside the scope of our model as discussed earlier. However, we can attempt to estimate the deviation from KdV as ι becomes small. We assume that by choosing m/n , we can still make q_0 small enough, but we need to account for the larger gradient of \hat{q} . First, we note that the only equation directly affected is the GB condition (24c). Then from the expansion of \hat{q} in (33), we find that the change in the flux surface $\Delta\psi$ can no longer be treated as linear in η . Allowing for quadratic terms in η through a small correction term $C^{(1)}\eta^2$ in (33), we get

$$\hat{q} \approx q_0 + \epsilon q_1 \eta (1 + C^{(1)}\eta). \quad (43)$$

Treating $C^{(1)}$ as a subsidiary expansion parameter, such that

$$\eta = \eta^{(0)} + C^{(1)}\eta^{(1)} + \dots, \quad (44)$$

we now find that the consistency of the KBC and the GB equations can be satisfied approximately to lowest order in $C^{(1)}$ by setting

$$q_1 \approx q_0 + O(C^{(1)}), \quad -\frac{\eta^{(0)}}{(1 + q_0^2)} = A_{,\xi}, \quad \eta^{(1)} = -\left(\eta^{(0)}\right)^2. \quad (45)$$

Note that due to the $O(C^{(1)})$ term in $q_1 - q_0$ is formally much larger than the $O(\epsilon)$ correction term, the optimum shear is no longer localized to a particular value as in the KdV case (39).

As shown in Appendix B subsidiary expansion leads to the Gardner's equation [33, 62]

$$\partial_t B + 6(B + c_1 C^{(1)} B^2)\partial_x B + \partial_x^3 B = 0, \quad (46)$$

where c_1 is a constant. Due to the additional B^2 term in the Gardner's equation (46) compared to the KdV equation (41), under the TW ansatz we need to replace the cubic f^2 in (42) by a quartic [33]. Therefore, we need four roots to describe B in this case, either all real, or two real and a pair of complex conjugates.

B. Extension of the slab geometry results to general toroidal geometry

To describe the region near the axis, which cannot be done within the slab model, we turn to the NAE theory.

On the magnetic axis, B is a constant. From first-order NAE, we find that in the immediate vicinity of the axis, $(\partial_\ell B)^2$ is quadratic in B , with B varying within the roots B_m and B_M . The description of B within the second-order NAE theory agrees completely with the cubic or the KdV picture we obtained in the slab limit. In particular, we recover the cubic formula (42) for $(\partial_\ell B)^2$ with three real roots (B_m, B_M, B_X) . Any corrections to (42) is higher order in the NAE picture. We will discuss in detail the NAE predictions for the roots B_M, B_m, B_X in Section V. The major drawback of the NAE theory is that the effect of shear is missing since it appears only in higher orders. Thus, the description of B_X , which depends crucially on the shear, is incomplete.

To include the effect of shear, we now go beyond the NAE limit and extend the free-surface idea proposed earlier in the slab model to more general geometries. We seek geometries in which the dependence on the fast variation is straightforward. Such a case arises with a large-aspect-ratio torus with nearly circular flux surfaces. Instead of the Cartesian coordinates, we shall now use the Clebsch coordinates $(\psi_s, \alpha_s, \Phi_s)$, where the subscript denotes the surface around which we carry out the surface expansion. In these NAE Clebsch coordinates, we have

$$\mathbf{B}_s = G_0 \nabla \Phi_s, \quad \mathbf{B}_s = \nabla \psi_s \times \nabla \alpha_s \quad (47)$$

Similar to the slab geometry case, we assume a characteristic length L along both α_s, Φ_s , h along ψ_s and a maximum deviation a of the free-surface from the predicted NAE boundary. The various quantities are related to each other through the same slab geometry relations (25) and (26). Associated with the small correction to the boundary is a small amplitude correction to the potential Φ_s such that

$$\Phi = \Phi_s + \epsilon \varphi. \quad (48)$$

For vacuum fields, Boozer coordinates are semi-orthogonal since constant Φ_s surfaces are orthogonal to ψ_s, α_s as seen from (47) but $\nabla \psi_s \cdot \nabla \alpha_s$ is nonzero, in general. In Appendix C 1, we first assume complete orthogonality to make the calculations simpler and closer to the slab geometry. However, since the local shear and global shear are related to the non-orthogonality of ψ_s and α_s , it is crucial to account for it. Therefore, we relax the orthogonality later in Appendix C 2. We find that the non-orthogonality does not affect the calculations within the required order of accuracy. The assumption that the dependence on the fast variable is negligible requires that $|\nabla \psi_s|, |\nabla \alpha_s|, B_s$ do not vary appreciably from their mean values within the surface expansion region on the scales of interest. This limitation will be addressed in a subsequent publication on multiscale NAE theory.

The calculation parallels that for the slab geometry with the above assumptions except for minor technical differences. The slight differences from the slab geometry follow from the fact that the lowest order B is a

constant in the slab geometry, which is not the case in general geometry. As a result, the expressions for H are different. Therefore, we leave the details to Appendix C. Assuming second-order NAE near in the core provides a reasonably accurate description of QS in the inner region, we can perform a surface expansion to correct for the missing length scale associated with shear in the outer region. The overdetermination problem of QS can then be solved perturbatively. In the inner region, the solution is achieved through second-order NAE. In the outer layer, the compatibility condition between QS and the force balance leads to a unique value of the shear.

In summary, the perturbative approach to solving the overdetermined vacuum quasisymmetric system leads to the following results. First, we can show analytically that the compatibility condition between force balance and QS determines the rotational transform profile. Within our approximate model, we are able to show that the compatibility implies that for a given average rotational transform, there is a preference for an optimal shear. In fact, recent work [36] has shown that stellarators with precise levels of QS that can be derived from the Landreman-Paul precise QA indeed have an optimal shear for the best QS. We discuss this further in Section VI (see Fig. 5). Second, the functional form of $(\partial_\ell B)^2$ is not arbitrary. In general, it is cubic in B , which leads to the KdV equation for B . For small ι and $N = 0$, $(\partial_\ell B)^2$ is a quartic, leading to Gardner's equation for B .

IV. THE CONNECTION OF QS TO INTEGRABLE PDES: PAINLEVÉ PROPERTY

In the previous Sections, we established using perturbative techniques that QS is intimately linked to the KdV equation. In this Section, we take a non-perturbative route to show that the QS-KdV connection can be made using only three fundamental properties of B as discussed in Section II. First, physical quantities such as B, ψ will be assumed to be analytic and single-valued functions of their arguments. Second, B must satisfy the periodic boundary condition (11) in ℓ on a flux surface with a period $L(\psi)$. Third, \mathbf{u} must be such that a nontrivial special frame exists where B is α independent.

We note that the first assumption is physically reasonable, has been shown to hold near the axis [17], and is also borne out by extensive computations. The second assumption is an essential requirement for QS. Both of these assumptions do not apply to omnigenity. Regarding the third assumption, an alternative is to demand that B must satisfy the fundamental TW condition (6) everywhere on the flux surface. The third condition leads to an infinite number of field-line α -independent integrals of the form (17). In the perturbative approach, in addition to these assumptions, we also made certain assumptions on the geometry to make analytical progress with the force balance condition.

Before we proceed with our analysis, let us discuss some of the important known exceptional cases of QS. As stated earlier, the case with an exact symmetry (axisymmetric or helically symmetric) is a special case of QS because \mathbf{u} is determined independently of \mathbf{B} . The third condition, or equivalently $\mathbf{u} \cdot \nabla \mathbf{B} = 0$, is satisfied identically for every choice of $f(B, \psi)$ in the $\partial_\ell B$ equation (10). We find a similar degeneracy in approximate QS near axisymmetry [19, 63, 64], where no constraints exist on $\partial_\ell B$. The near-axisymmetric devices can not be made quasisymmetric to all orders and have higher symmetry-breaking errors than the Landreman-Paul precise QA. A more general analysis shows that in configurations that are not close to either axisymmetry or helical symmetry, the degeneracy is avoided, and $\partial_\ell B$ is once again constrained [65]. We shall also exclude the exceptional case of zero rotational transform [66] since we focus only on irrational surfaces while assuming continuity on rational surfaces. We shall return to the comparison with the axisymmetric case at the end of this Section.

Our main goal is to study the single-valuedness of B on a constant flux surface ψ that satisfies the $\partial_\ell B$ equation (10) and the $\partial_\alpha B$ equation (12), subject to the periodicity condition (11). Starting with the pioneering work by S. Kovalevskaya [67] on rigid body dynamics, the study of single-valuedness and singularities of differential equations in the complex domain has yielded fundamental results in several physics problems from quantum field theory to optics [68]. Extending from the real to the complex plane is a helpful technique that physicists often utilize in solving linear problems. However, as Kovalevskaya showed, going to the complex plane and analyzing singularities of highly nonlinear systems can be equally insightful. Moreover, singularities in the complex plane determine and control the behavior of analytic functions in the real line. An important example of this is a doubly periodic elliptic function [69, 70] whose singularities determine its periodicity on the real line. Our investigation is primarily motivated by the observation that the hidden symmetry of QS could admit a special Kovalevskaya-like solution [40].

We first shift to the TW frame where B is α independent, and the $\partial_\ell B$ equation can be treated as an ordinary differential equation (ODE) in ℓ with period $L(\psi)$. Since B is assumed to be a real analytic function of ℓ on the real interval $(0, L)$ with a nonzero radius of convergence, we can extend it to a complex analytic function $\mathcal{B}(\mathcal{Z})$ inside the disk $|\mathcal{Z}| < L$ with \mathcal{Z} denoting the complex ℓ . To be precise, we shall now demand that \mathcal{B} be a single-valued complex function of \mathcal{Z} , such that it has the same value at every point independent of the path along which it is reached by analytic continuation.

To proceed further, we need critical ideas from the well-developed theory of complex ODEs [67, 69, 71]. In contrast to solutions of linear ODEs, whose singularities are determined by those of the coefficients, nonlinear ODEs allow *movable* singularities, which depend on the

initial conditions. The standard example is $y' + y^2 = 0$, whose general solution, $y = (x - x_0)^{-1}$, depends on the integration constant x_0 determined by the initial condition $y(0) = -x_0^{-1}$. The possible singularities of ODEs are known. They include poles, branch points, essential singular points, and essential singular lines. Single-valuedness of functions breaks down near *critical singularities*, such as branch points of algebraic or logarithmic nature. If the critical singularities are fixed, the functions can be made single-valued by defining suitable branch cuts or fixed Riemann surfaces. However, the presence of singularities, which are both critical and movable, leads to dense multi-valuedness around movable singularities of solutions and nonintegrability ([67, 72] and references therein). The absence of movable critical singularities in the general solution of an ODE is called the *Painlevé property* (PP) of an ODE.

We now recall some classical results on ODEs with the PP (details given in [67, 69, 71]). Let us rewrite the $\partial_\ell B$ equation in the complex plane as

$$\mathcal{B}'(\mathcal{Z}) = \mathcal{F}(\mathcal{B}(\mathcal{Z})). \quad (49)$$

The only first-order ODE of the first degree that possesses the PP is the Riccati equation, where \mathcal{F} is quadratic in \mathcal{B} . For first-order ODEs of degree $n > 1$, the equations of the form

$$\mathcal{B}'(\mathcal{Z})^2 = P_m(\mathcal{B}(\mathcal{Z})) \quad (50)$$

with P_m a polynomial of degree m possess the PP provided $n \leq 2m$. Furthermore, only four possibilities exhaust all ODEs of the form (50). With suitable variable transformations, all of them can be reduced to the following ODE with a cubic nonlinearity

$$\mathcal{B}'(\mathcal{Z})^2 = P_3(\mathcal{B}(\mathcal{Z})), \quad (51)$$

which is exactly solvable in terms of elliptic functions and their degenerate cases. As is well-known, elliptic functions are doubly-periodic, meromorphic functions. The dependence on the arbitrary initial condition or the TW frame thus leads to only movable poles and no movable critical singularities. Hence, the solution possesses the PP. These classical results follow from standard Painlevé test and extensions of Malmquist's theorem [69, 73]. They show how stringent and rigid the constraint of single-valuedness can be.

Returning to the QS problem, we first observe that the Riccati equation for B is inconsistent with the NAE solution. The Riccati equation for B will have constant real coefficients on a flux surface, which does not admit nontrivial periodic solutions on the real line [74]. As discussed in Section III A and III B the perturbative treatment near the slab or the axis shows that $(\partial_\ell B)^2 = P_3(B), P_4(B)$ is more appropriate, which coincides with two of the four forms of ODEs of first order and second degree with PP. The periodicity condition can be easily satisfied with the elliptic functions for these cases.

Now, the cubic and quartic polynomials are the twice-integrated forms of the KdV and Gardner's equations. The PP of the KdV and Gardner's equation in the TW frame is well-known and is conjectured to be essential for integrable PDEs with soliton solutions [75, 76].

We would now like to address whether PP is necessary and sufficient for a quasisymmetric B . It is certainly sufficient for QS since both the triple product form (8) and the periodicity condition can be satisfied. However, the necessity is not apparent, particularly in light of axisymmetry, where no such stringent restriction on $\partial_\ell B$ appears. In axisymmetry, weak singularities such as $R^m \log R^n$, with integer m, n often arise in the description of ψ [77] and in B in cylindrical coordinates. However, these singularities are fixed and, therefore, not of the critical movable type. To further understand the difference between a perfectly axisymmetric system and a system with excellent but not exact QS, we need to look deeper into the $\mathbf{u} \cdot \nabla B = 0$ condition. As discussed in Appendix A, if QS were exact, we would have the same characteristics as axisymmetry. However, unlike the axisymmetric problem, the QS problem is intrinsically overdetermined and three-dimensional. With this in mind, we shall now motivate the PP as a criterion that allows one to look for robust quasisymmetric systems.

In axisymmetry, the geometry and the B decouples. Thus, all field lines are equivalent, and the TW frame, where $H = 0$, is the same for all α . Regarding the effect on the singularities, this implies that the dependence of B on the field line label is precisely the same for each singularity, which amounts to a trivial rigid shift of frame. However, in a generic approximate 3D QS, the geometry and B are strongly coupled. Due to the overdetermined nature, the $\mathbf{u} \cdot \nabla B = 0$ condition can only be approximately satisfied. As a consequence, the TW frame $H = 0$ is, in general, different for different field lines. Thus, the α dependence of the singularities of $\partial_\ell B$ will vary from field line to field line. Since these movable singularities can be critical, single-valuedness of B will be harder to achieve. However, when we demand the PP, the moving singularities are not critical, which respects the single-valuedness of B . As will be shown in Sections VI and VII, every numerically optimized quasisymmetric stellarator has the PP. Furthermore, as the optimization progresses, the PP property emerges quickly and is maintained. Therefore, we can argue that the PP is necessary and sufficient for obtaining robust QS in a 3D stellarator using numerical optimization methods, where single-valuedness and periodicity of B are enforced directly using a Fourier representation.

Finally, we note that none of the above arguments required knowledge of the exact force balance condition. From the perturbative calculations, we expect that force balance determines the optimal shear profile. The roots of the polynomial can vary with the flux surface label, and force balance determines their profiles.

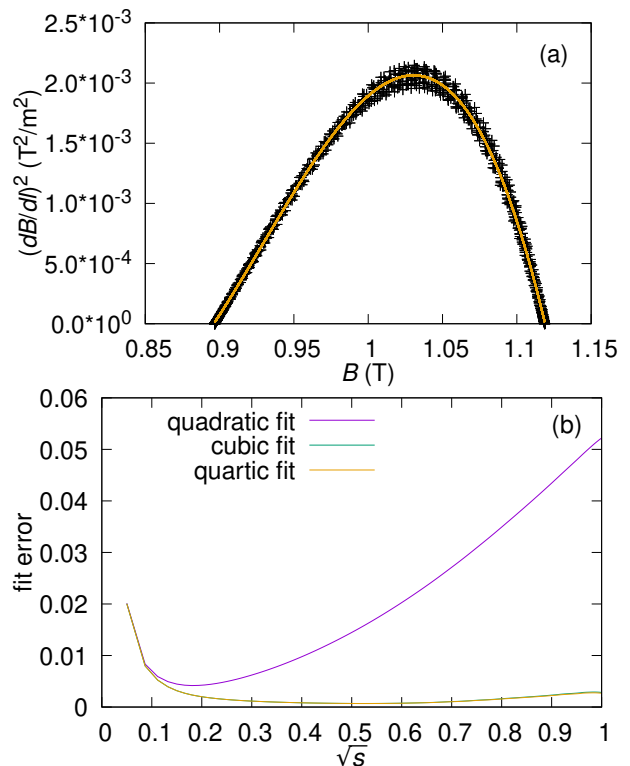


FIG. 1. The value of $(dB/dl)^2$ on the outermost flux surface in the precise QA equilibrium [4] is plotted as a function of B , alongside a cubic polynomial fit in (a). In (b), the errors of quadratic, cubic, and quartic fits are compared on each flux surface, demonstrating that a cubic ansatz (as predicted by KdV) is sufficient. Hence, precise QA has the Painlevé property for B .

V. REDUCED DIMENSIONALITY OF QUASISYMMETRIC B

In the previous Section, we have shown that $(\partial_\ell B)^2$ is a cubic or quartic polynomial in B , whose roots can only be functions of ψ . Therefore, the PP significantly reduces the dimensionality of quasisymmetric B , which we shall now fully explore. We shall restrict ourselves to the cubic or the KdV case since that was shown in the perturbative approach to lead to better force-balance.

With the TW constraint, the twice integrated KdV equation can be written as

$$\left(\frac{\partial B}{\partial \ell}\right)^2 = \mathcal{D}(\psi)(B_M - B)(B - B_m)(B - B_X), \quad (52)$$

where the roots of the cubic polynomial, $B_i = \{B_M, B_m, B_X\}$, are functions of ψ , and $\mathcal{D}(\psi)$ is a proportionality factor. The exact solution of (52) subject to the periodicity constraint (11) can be expressed in terms of elliptic functions [9, 30].

To obtain the proportionality factors between (x, t) and (l, α) explicitly, we now proceed from (52) and de-

rive the KdV equation. Differentiating (52) twice with ℓ and using the $\partial_\alpha B$ equation (12) we get (41), the KdV equation for B . Here, the coordinates (x, t) are defined in terms of (α, ℓ) as

$$\frac{x}{\ell} = \sqrt{\frac{\mathcal{D}}{2}}, \quad \frac{t}{\int d\alpha H} = \frac{\sqrt{\mathcal{D}/2}}{2(B_M + B_m + B_X)}. \quad (53)$$

The $\partial_\alpha B$ relation (12), now takes the following form of a 1D traveling wave equation with speed $c(\psi)$,

$$\frac{\partial B}{\partial t} + c(\psi) \frac{\partial B}{\partial x} = 0, \quad c(\psi) = 2(B_M + B_m + B_X). \quad (54)$$

B is then obtained from the cnoidal solution [30] of KdV,

$$B = B_m + (B_M - B_m) \text{cn}^2 \left(\sqrt{\frac{B_M - B_X}{2}} (x - ct), m \right),$$

$$m = \frac{B_M - B_m}{B_M - B_X}, \quad 0 \leq m \leq 1. \quad (55)$$

Here, $\text{cn}(u, m)$ is the Jacobi cosine elliptic function with modulus m . B varies between B_m and B_M . The period of B , $L(\psi)$, diverges logarithmically as $m \rightarrow 1$. One would expect this behavior near a separatrix, where periodicity along a field line is lost because the field line cannot cross the X-point. In particular, it is interesting to note that in the $m \rightarrow 1$ limit, B takes the form of the infinite KdV soliton (reflectionless potential). The adiabatic invariant and integrals of the form (17) obtained from KdV potentials are manifestly time (α) independent [38, 39, 78].

We first note that on any flux surface ψ , we have four flux functions that determine B , namely \mathcal{D} and B_M, B_m, B_X , the three real roots of the cubic polynomial in (52). However, as shown in Appendix D, \mathcal{D} can be expressed in terms of the rotational transform ι and the roots. Therefore, the connection with KdV points to a hidden low-dimensionality of the description of B .

The functions B_M and B_m denote the maximum and minimum values of B on a flux surface, respectively, and B_X is a third root of the polynomial. The extrema of B , given by B_M and B_m depend only on ψ , which implies that they can be straightened out using straight field line coordinates. The behavior of B in Boozer coordinates is well known [17, 18, 27] near the magnetic axis and is consistent with (52). On the axis B is a constant, B_0 , and varies as $B \approx B_0(1 + \bar{\eta}\sqrt{2\psi} \cos \vartheta) + 2\psi(B_{20} + B_{22} \cos 2\vartheta)$ near the axis. Here, ϑ is the well-known Boozer angle [27]. The constant $\bar{\eta}$ dominates the maximum variation of B on a flux surface, with the $O(2\psi)$ term being only a small second-order correction. Within the NAE framework, B_X and \mathcal{D} are constant throughout the volume, with $\mathcal{D} \propto ((\iota - N/M))^2$. The NAE predictions are

$$\frac{B_M}{B_0}, \frac{B_m}{B_0} = 1 \pm \bar{\eta}\sqrt{2\psi}, \quad \frac{B_X}{B_0} = \frac{4B_{22}/B_0 + \bar{\eta}^2}{4B_{22}/B_0 + 2\bar{\eta}^2}. \quad (56)$$

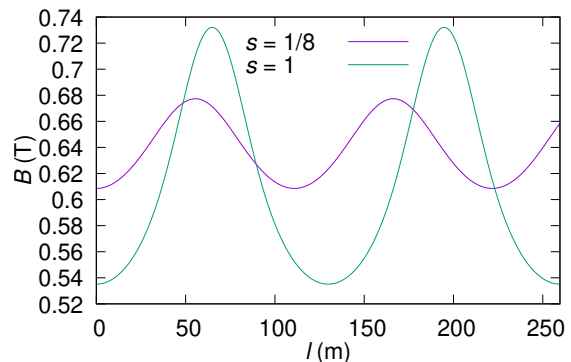


FIG. 2. The value of B in a quasisymmetric device in the core ($s = 1/8$) and at the edge ($s = 1$). The separatrix is outside of the device but close to its edge. Note the increasing period as the separatrix is approached.

Since $B_{22}, B_0, \bar{\eta}$ are all constants related to the B spectrum in Boozer coordinates, the NAE prediction (56) for the third root is a constant. However, as shown earlier in Section III A, the third root depends on the rotational transform and, hence, the shear profile. Thus, the NAE predictions are accurate only when the rotational transform is effectively constant. The limiting surface where $m \rightarrow 1$ corresponds to $B_X \rightarrow B_m$ is the separatrix. We can use (56) to approximately predict its location.

VI. NUMERICAL VERIFICATION

We shall now demonstrate numerically that a large class of quasisymmetric B satisfies the integrated form of KdV as given in (52). As demonstrated in Fig. 1(a), $(dB/dl)^2$, when plotted as a function of B , has the form of a cubic polynomial in the precise QA equilibrium [4]; the scatter is due to imperfect QS. On the other hand, Fig. 1(b) shows that increasing the polynomial order beyond three does not lead to an observable decrease in error (defined as $1 - r^2$, where r^2 is the coefficient of determination), as the fit error is dominated by QS error. Thus, Fig. 1 supports equation (52) as a model for a device with perfect QS. A similar analysis for other configurations, which tend to have more QS error, is shown in Appendix E. (Note that s is the normalized toroidal flux in all figures.)

In Fig. 2, we demonstrate that B appears roughly sinusoidal far from the separatrix but becomes soliton-like (sharper peaks, flatter troughs) as the separatrix is approached. Note that the B shown in Fig. 2 is perfectly quasisymmetric, as symmetry-breaking modes have been filtered out. The period of B increases as $L(\psi) \rightarrow \infty$ on the separatrix.

With the global description of the exact quasisymmetric B , (55), at our disposal, we now investigate a key element of this theory: the physical meaning of the roots

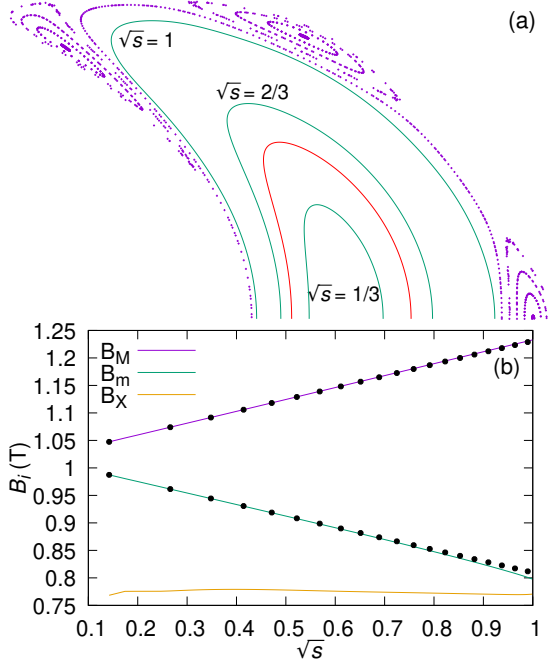


FIG. 3. Prediction of maximum toroidal volume that can be made quasisymmetric in precise QA. The boundary of the extended precise QA and two other flux surfaces are shown inside a Poincaré plot of the islands in (a), and the roots are plotted in (b). The boundary of the original precise QA is shown in red. Note that the islands occur where the second and third roots touch approximately.

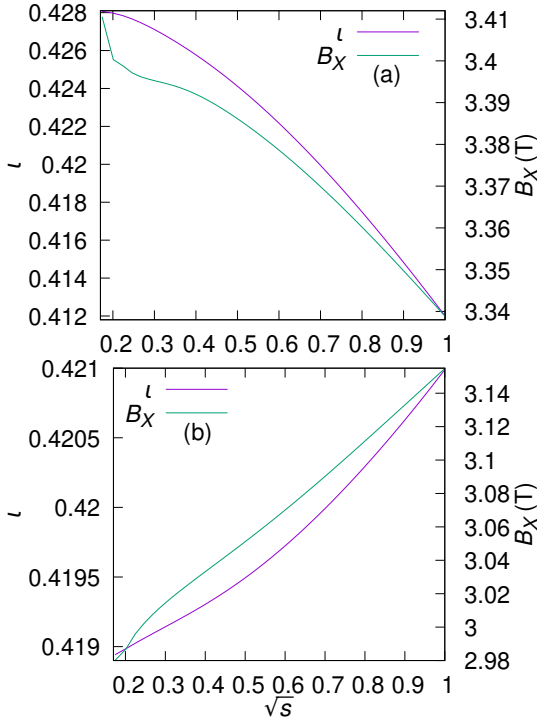


FIG. 4. The B_X and ι profiles plotted for precise QA versions with negative shear (a) and positive shear (b).

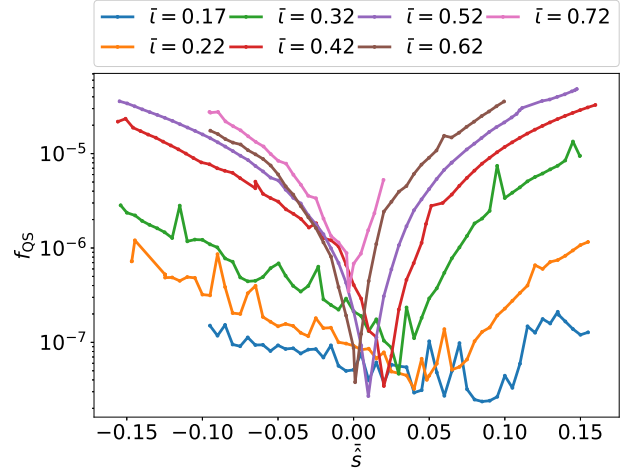


FIG. 5. Radially-summed two-term QS error, f_{QS} , plotted against average shear \bar{s} for different average rotational transforms, $\bar{\iota}$. The quasisymmetry error is summed over the $s = \{0.0, 0.1, \dots, 1.0\}$ surfaces. The definitions of the ι and \bar{s} averages are given in (57). Note the V-shaped plots indicating a sharp change in f_{QS} around a preferred \bar{s} for a particular $\bar{\iota}$, as predicted by our slab-geometry model. Note also the loss of preference for any particular \bar{s} as $\bar{\iota}$ becomes smaller.

B_i . In Fig. 3(b), we show the typical behavior of the roots. Symmetry-breaking modes have been filtered out, and the roots are obtained by a cubic fit of the numerical data. Points represent the actual minimum and maximum values of B on each flux surface. Surprisingly, the NAE description of B_M and B_m continues to hold even far from the axis. The third root B_X depends quite sensitively on the ι profiles (Fig. 4). We show in Fig. 4 that for small but finite shear, B_X tracks the ι profile quite closely but varies more for positive shear. This is in accordance with our free-surface approach to QS, which showed that B_X must be a function of the shear parameter.

The question of why quasisymmetric devices with excellent QS, such as the Landreman-Paul solution, have a small but finite magnetic shear is important to understand both for theoretical and practical reasons since shear controls MHD stability. However, NAE for QS is not very helpful when it comes to shear, as we discussed earlier. We shall now present an explanation based on the insight from the slab geometry model and through optimization with target shears. In Fig. 5, we show how the quality of QS f_{QS} depends on the average shear for a given average rotational transform. The average shear is computed by fitting a line to the ι profile

$$\iota(s) \approx \iota_0 + \iota_1 s, \quad \bar{s} \equiv -\iota_1/\bar{\iota}, \quad (57)$$

where $\bar{\iota}$ is the average of the actual ι profile. Since these QS devices have very low shear, this definition suffices. From an optimization point of view, asking for a specific \bar{s} for a specific average ι will generally lead to degradation

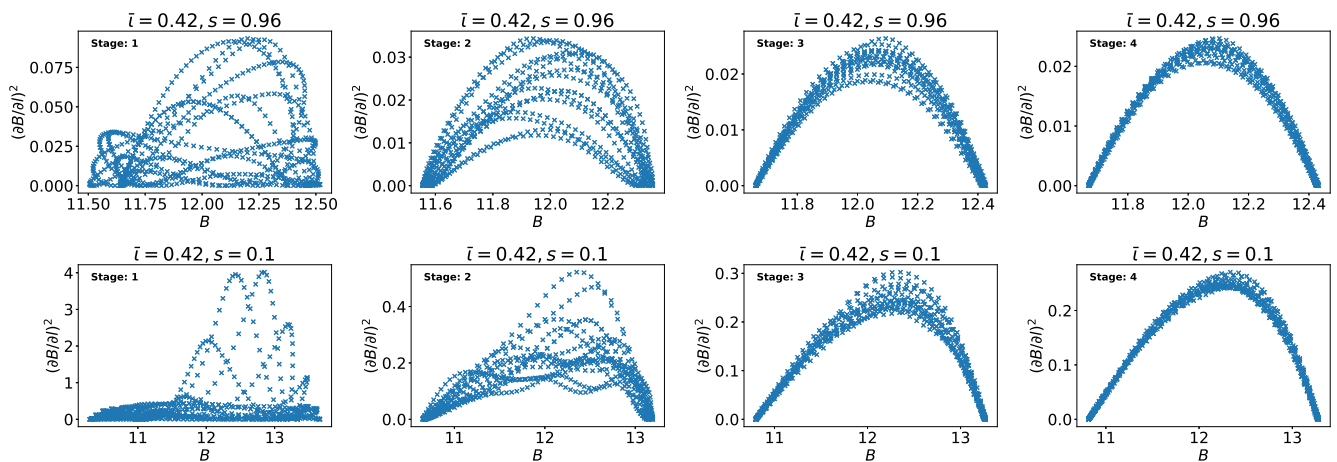


FIG. 6. $(\partial_t B)^2$ as a function of B , on two surfaces, across the four stages of optimization for the Landreman-Paul precise QA configuration.

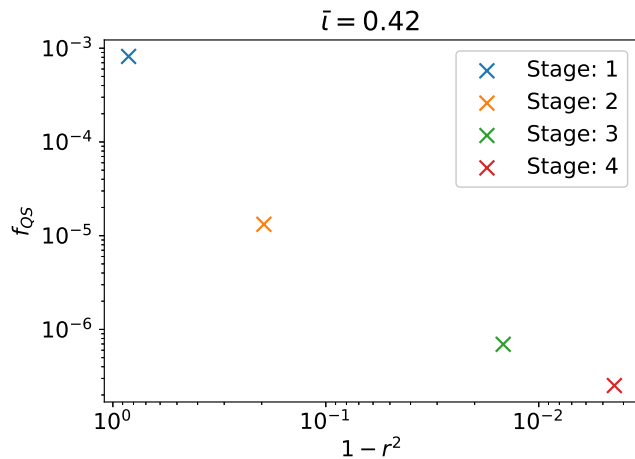


FIG. 7. The two-term QS error, summed over the surfaces, is plotted on the ordinate against $1 - r^2$ (averaged across all surfaces) on the abscissa, where r^2 is the coefficient of determination for a cubic best fit.

in the QS quality because of the extra shear constraint. However, from the sharpness of the V-shaped plots in Fig. 5, we observe that QS seems to have a strong preference for a particular \hat{s} for a given $\bar{\iota}$, particularly in the range of $\bar{\iota} \geq 0.32$. For lower values of $\bar{\iota}$, the V-shape flattens out. In light of the slab-geometry model, we can explain this feature as a direct consequence of the overdetermination problem. The force balance and the QS condition can only be satisfied simultaneously for a narrow range of shear around a preferred value of ι that is not too small.

Next, we demonstrate how we can estimate the maximum volume that a quasymmetric field can occupy only from B properties for any geometry. From the analytical solution for B (55), we find that the periodicity of B is

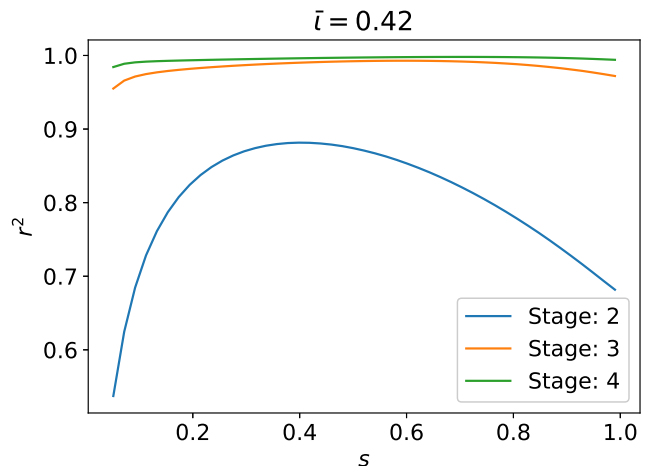


FIG. 8. For a cubic best fit, we plot the coefficient of determination against the surfaces of the Landreman-Paul configuration across the latter three stages of the optimization.

maintained as long as $0 \leq m < 1$. As we saw earlier, the limit ($m \rightarrow 1, B_m \rightarrow B_X$) was the limit in which the connection length diverges. Using the simple NAE estimates for the roots B_m and B_X , we can estimate where the two roots will intersect, thereby signaling the breakdown of periodicity. We have demonstrated in Fig. 3 how this estimate can predict the maximum volume of nested surfaces in precise QA extended using coils developed recently [79]. The appearance of the island chain in Fig. 3 is due to the failure of QS (which guarantees nested flux surfaces [22]) and not due to a resonance with the helicity of the QA [80].

Lastly, we show how the integrated form of KdV is approached through the stages of optimization, where the parameter space is progressively expanded. In Fig. 6, for

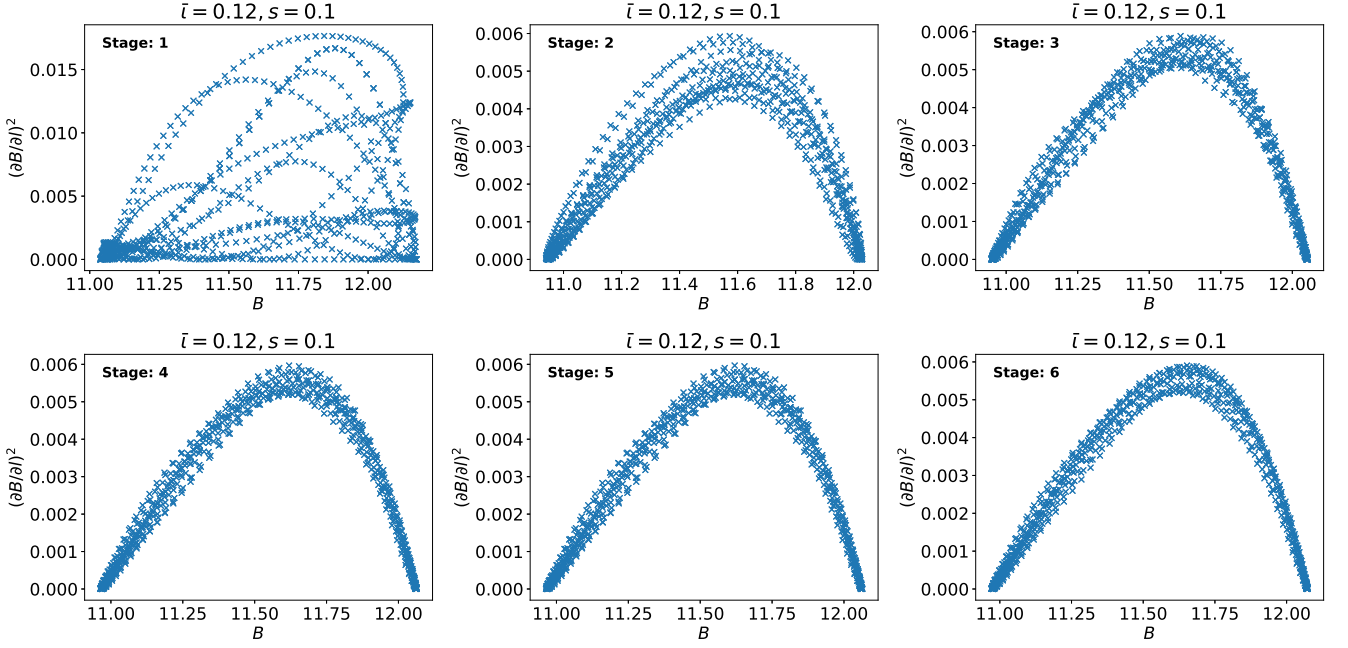


FIG. 9. $(\partial_t B)^2$ as a function of B , for $s = 0.1$, across the six stages of optimization for the $\bar{\iota} = 0.12$ Buller configuration.

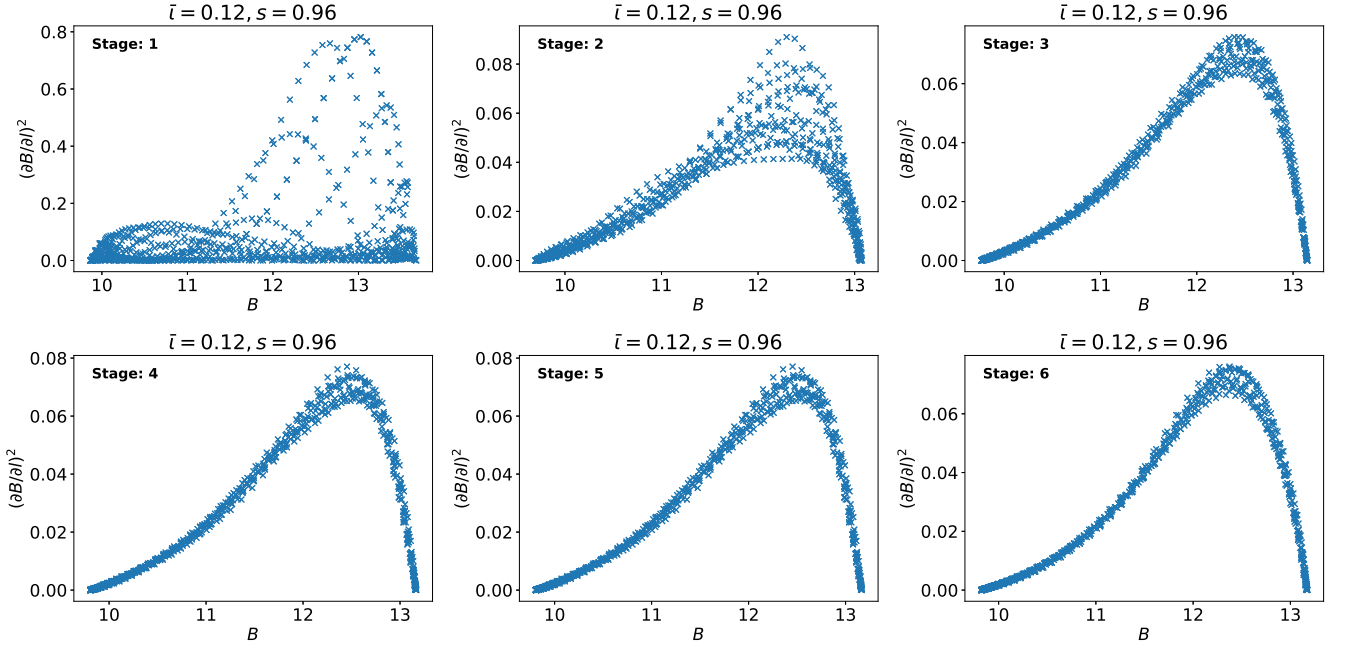


FIG. 10. $(\partial_t B)^2$ as a function of B , for $s = 0.96$, across the six stages of optimization for the $\bar{\iota} = 0.12$ Buller configuration.

the Landreman-Paul precise QA configuration, not only does the ‘noise’ decrease (as expected from improving QS), but the shape gets increasingly cubic. We show this both for a surface close to the axis and a surface close to the edge. Figures 7 and 8 further show how the KdV integrated cubic increases in accuracy (as determined by the coefficient of determination) further into the opti-

mization process. In Figures 9, 10, 11, and 12, we show similar plots for the low mean rotational transform Buller configuration; note that the trend is towards quartic instead of cubic. As evident from these plots, the PP is established in the entire volume within the very first few stages of optimization and is maintained thereafter.

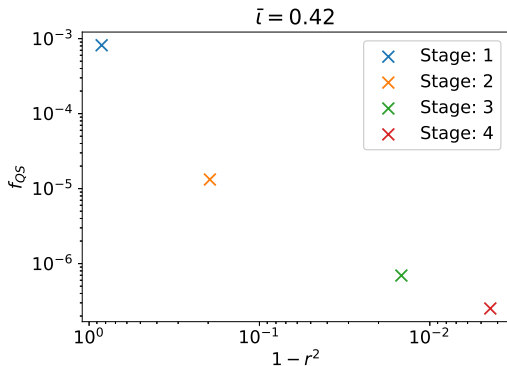


FIG. 11. The two-term QS error, summed over the surfaces, is plotted against $1 - r^2$ (averaged across all surfaces), where r^2 is the coefficient of determination for a quartic best fit.

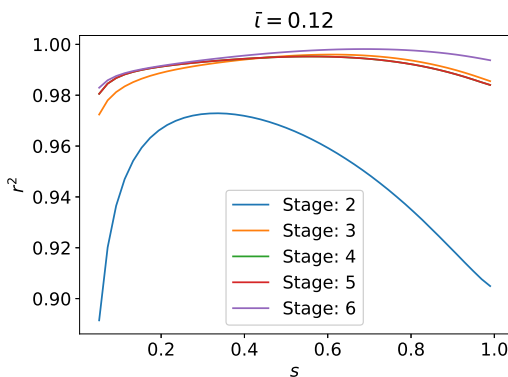


FIG. 12. For a quartic best fit, we plot the coefficient of determination against the surfaces of the Landreman-Paul configuration across the latter five stages of the optimization.

VII. DATA DRIVEN VERIFICATION

We have put forth several analytical arguments in favor of the connection between QS and the well-known integrable PDEs, KdV, and Gardner’s equation (for small rotational transforms). Our analysis so far has been based on NAEs, an approximate slab geometry model calculation and its extensions to more realistic geometries, and finally, soliton theory. We have also demonstrated numerically good agreement with several configurations with good QS. In this Section, we take a different approach based on data-driven techniques to determine the underlying system of equations describing quasisymmetric B on a flux surface. Our primary tool is pySINDy [34, 35], which fits for governing differential equations and favors fewer terms to combat over-fitting.

We have primarily used the family of quasisymmetric VMEC equilibria generated in [36]. For additional verification, we considered further configurations from the QUASR database [37]. Henceforth, we

shall refer to them as the Buller and the Giuliani configurations. For the latter, configurations were selected with three representative mean rotational transforms. They were chosen to have the number of field periods, $N_{fp} = 2$, an aspect ratio close to six (to mirror the Buller configurations), and the lowest possible quasi-axisymmetry error (as defined in [37]).

Using the Buller configurations, we verified the quasisymmetry-imposed traveling wave form (12). We calculated $H = -\partial_\alpha B / \partial_l B$, taking $l = 0$ at $\phi = 0$ and considering one field period. The traveling waveform could then be verified by the fact that H was independent of l . Equivalently, we calculated $t = \int_0^\alpha d\alpha' H$ and plotted B on a surface parameterized by l and t , in which case equation (12) indicates that we should see traveling waves of unit speed. These results are presented in Fig. 13, where we can clearly see QS manifest as a traveling wave. With the traveling waveform, the PDE governing B reduces to ODEs, which pySINDy can easily determine. In fact, we also attempted to use pySINDy to identify PDEs directly, and could straightforwardly recover the traveling wave. Even in configurations with relatively substantial deviations from quasi-symmetry, the traveling wave structure is quite robust. Under the traveling wave assumption, the equations are reduced to ODEs anyway, so we focused on the ODE discovery problem. Future work can try to use pySINDy for PDE identification in regimes where significant deviations from traveling wave behavior are observed, which might require configurations quite far from quasi-symmetry.

Next, we use pySINDy to discover the underlying ODEs that govern B on a flux surface. To that end, a sequentially thresholded least squares algorithm [81, 82] was used for the fitting, with a cost function that promotes sparsity in the data fit. For each magnetic configuration’s flux surface, the B against l profiles of multiple field lines spanning the surface were used as training data. The quantity $(\partial_l B)^2$ on a flux surface was fit against a linear combination of terms from a ‘feature library,’ chosen here to be a selection of polynomial terms, with the model parameters as the coefficients. Since the KdV and Gardner’s equation, together with the traveling waveform, lead to cubic and quartic polynomials, using the polynomial basis in pySINDy was a natural choice. A range of models was produced at varying sparsity parameters; the models were then tested on data from magnetic field lines not used in the training data. For sparsity parameters that were too large, it was found that there was a sharp drop in the success of the fit as too many terms were dropped; we chose the pySINDy model before this drop in performance. This is a version of hyperparameter scanning to find the Pareto-optimal fit (optimal tradeoff of model complexity versus model accuracy) to the data.

In Fig. 14, we demonstrate the outcome of the pySINDy fit to $(\partial_l B)^2$ on a flux surface for three representative configurations. A cubic was a good fit for all the configurations on flux surfaces sufficiently close to the

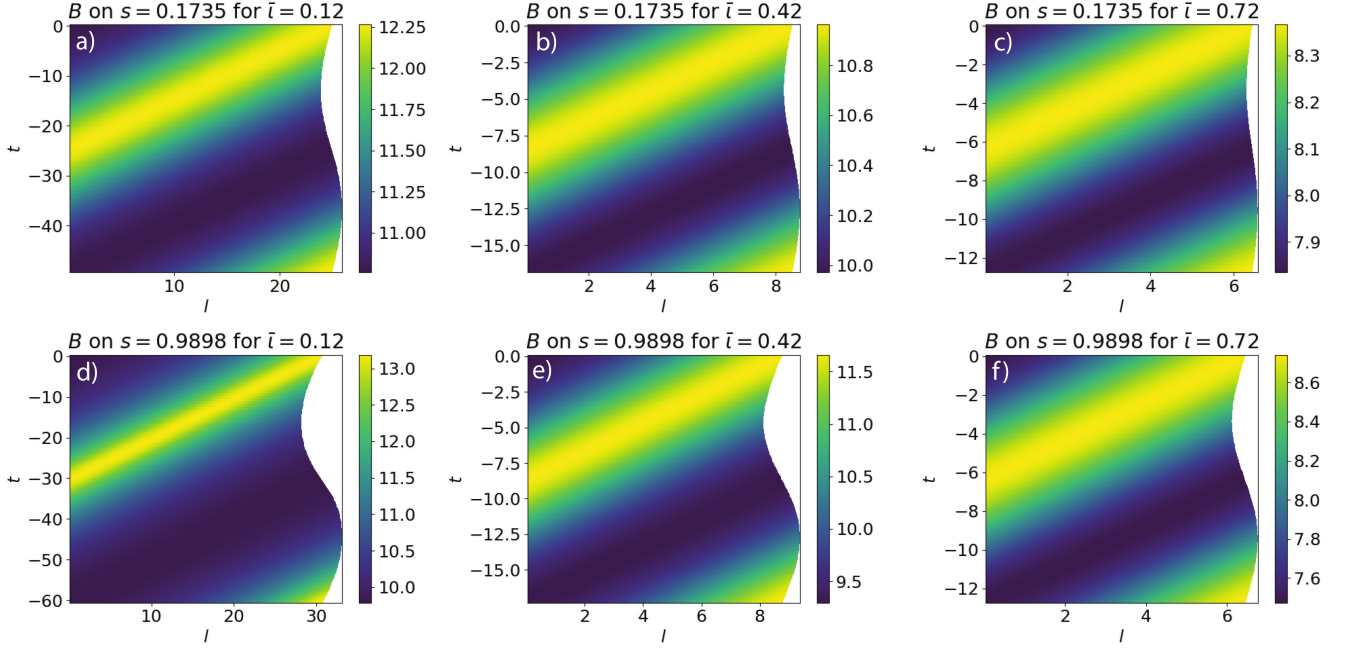


FIG. 13. B on a magnetic surface parameterised by l and t

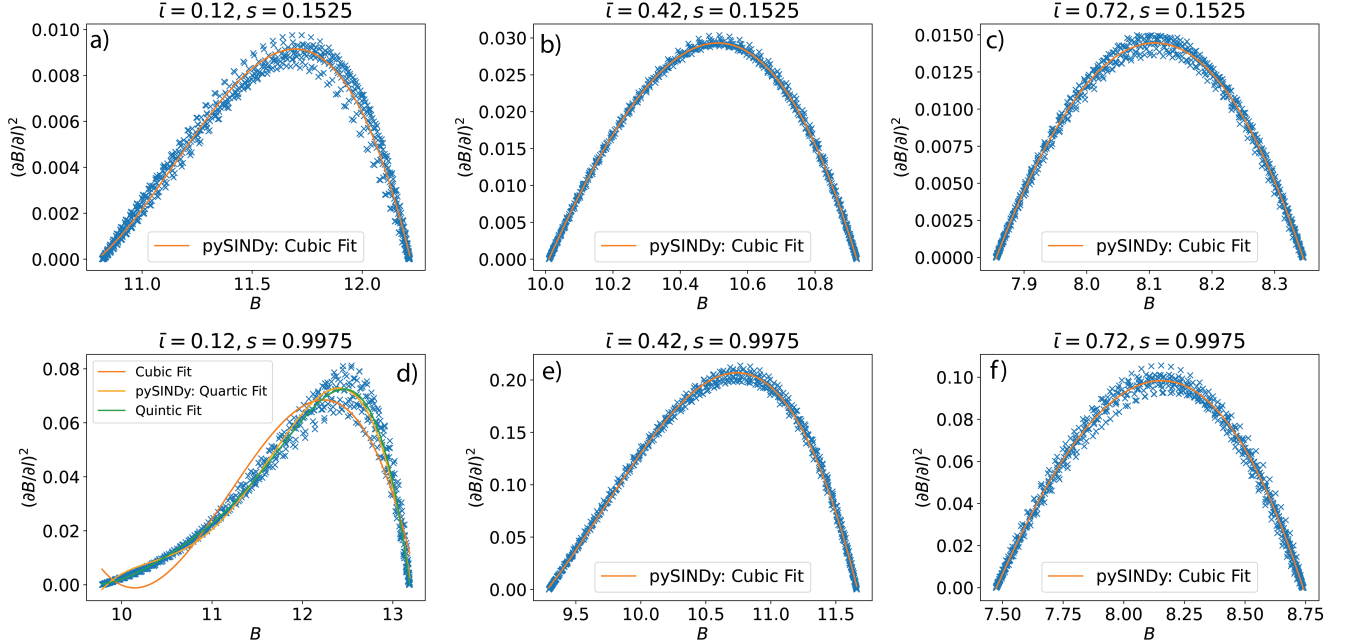


FIG. 14. $(\partial_t B)^2$ as a function of B on two surfaces, on configurations at three different mean rotational transforms. Only at low rotational transform and far away from the axis, as in d), is a cubic a poor fit.

axis, as expected from the NAE analysis. We see in Fig. 15 that the shapes from the Giuliani configurations are similar to those of the Buller configurations.

For configurations with low mean rotational transform, a cubic was no longer the best model on the outermost

surfaces (see Figures 16 and 17); pySINDy indicated that a quartic was an effective fit on such surfaces. We also see that a quintic performs well. However, within the error range, the benefit of using a quintic is very marginal compared to the quartic, as demonstrated clearly in Figs. 16 and 17. In Fig. 18, we see that the deviation from

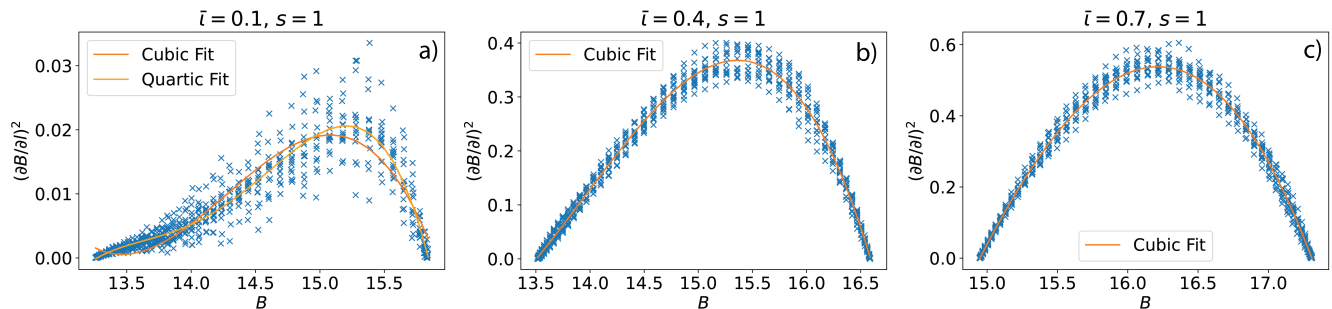


FIG. 15. $(\partial_\ell B)^2$ as a function of B on the outermost surface, on configurations at three different mean rotational transforms selected from the QUASR database. Only at low rotational transform and far away from the axis, as in a), is a cubic a poor fit.

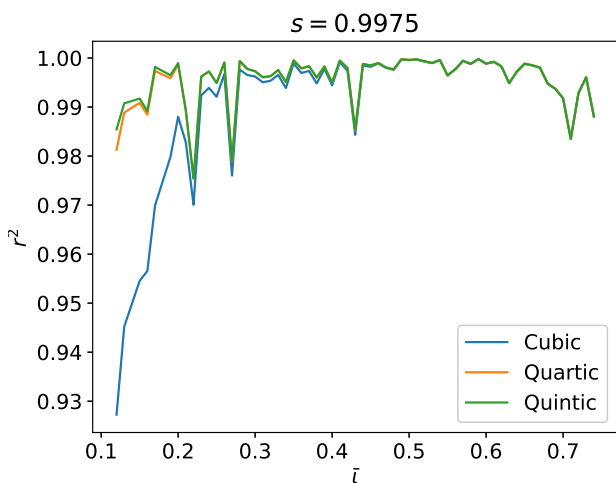


FIG. 16. The coefficient of determination on the outermost surface, for different parameterizations of $(\partial_\ell B)^2$ as a function of B , across the Buller configurations, where each configuration has a different mean rotational transform.

the mean from many pySINDy models generated by subsampling is small. This provides additional evidence that cubic models fit the data extremely well, except near the plasma boundary in low- ι configurations, for which a quartic correction is robustly picked up during model identification.

Finally, the evolution of the roots in the representative sample configurations and surfaces is shown in Fig. 19. For the cubic case described by KdV, there are three real roots, as we discussed earlier in Section VI. The case for low ι , described by Gardner's equation, on the other hand, can have two real and two complex conjugate roots owing to its quartic nature. In the leftmost panel of Fig. 19, we show the two real roots of the quartic $(\partial_\ell B)^2$ given by the maximum and the minimum of B on a flux surface s and the other pair of complex conjugate roots.

VIII. DISCUSSIONS

In summary, we have demonstrated that periodic soliton solutions of the KdV equation lead to a broad class of excellent quasisymmetric B . We have done so by employing three different approaches. In the first approach, we reformulate the QS problem as a free-surface problem. The inner (closer to the axis) solution is assumed to be the second-order NAE solution, which has been demonstrated to capture essential features of even low-aspect ratio practical designs. The outer free-surface solution is then constructed by considering the length scale over which the magnetic shear varies. We can perturbatively solve the overdetermination problem by ensuring compatibility of the force balance and the QS condition. Our results show that shear is constrained to have an optimum value by the overdetermination problem and the magnetic field strength. The field strength must also satisfy the KdV equation, a well-known integrable PDE. We can also obtain Gardner's equation for small values of the rotational transform.

In the second approach, we show that under three very general assumptions, namely, periodicity in ℓ , analyticity of B , and the existence of a nontrivial TW frame, we can motivate why QS naturally leads to the KdV or Gardner's equation for the magnetic field strength. The essential property is the Painlevé property, which ensures B stays single-valued. Several results follow from the connection between QS and the KdV equation.

Firstly, the description of a class of precisely quasisymmetric B can be reduced to understanding the behavior of the roots B_i of a cubic polynomial. These roots correspond to extrema or saddle points of B on a surface. In particular, B , which satisfies the periodic KdV equation, is the potential of the periodic Schrodinger equation where B_i 's are related to the endpoints of the band gap [9, 30]. Since the spectrum of KdV is time-independent, the roots do not depend on time. This confirms the well-known statement that the extrema or saddle points of B depend only on the flux label in QS [11]. Moreover,

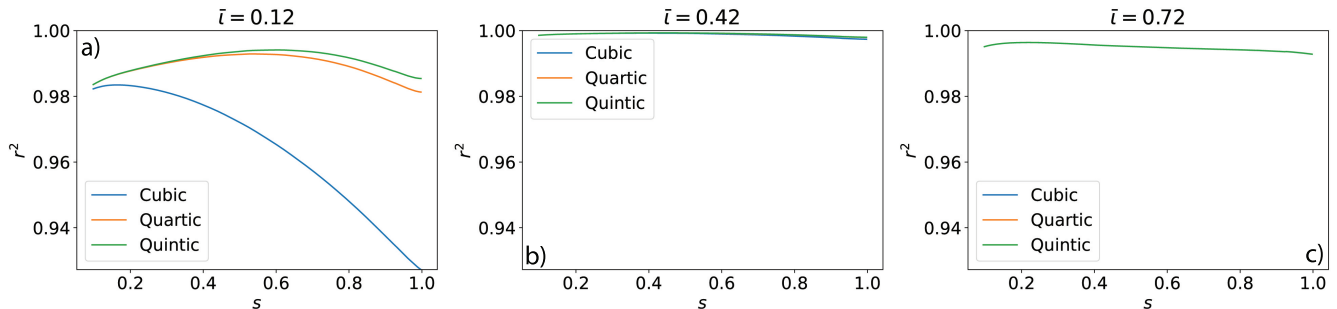


FIG. 17. The coefficient of determination as a function of the surface, for three different mean rotational transforms, for different parameterizations of $(\partial_t B)^2$ as a function of B .

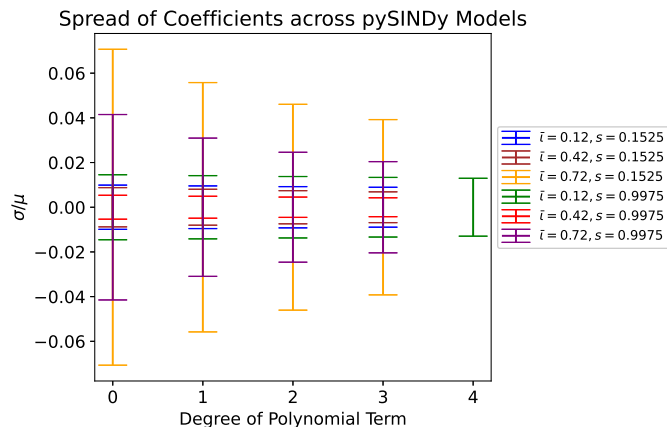


FIG. 18. 200 pySINDy models for each shown configuration and surface were produced, each which sampled, with replacement, 60% of 1600 available points on each flux surface. For each model, the standard deviation spread of the coefficients (normalized by the mean) is plotted.

the free-surface approach showed that B_X is a function of the shear. Therefore, the invariance of B_X on a flux surface effectively implies that the rotational transform $\iota(\psi)$ must be independent of the field line label (time). In other words, QS leads to an integrable field line Hamiltonian, which preserves nested flux surfaces [11]. Furthermore, since various aspects of the flux surface shaping can be deduced [12] from the Fourier coefficients of B , the hidden lower dimensionality is beneficial for understanding shaping. A similar hidden lower dimensionality is found in the description of the curvature of isodynamic magnetic field lines [28]. Once again, we emphasize that these hidden lower dimensionalities in the field strength or geometry are a direct consequence of the underlying soliton dynamics: the KdV equation in the case of QS and VFE in the case of isodynamic fields.

Secondly, the hierarchy of quasisymmetric invariants, as given by (17), can be understood in terms of the hierarchy of the conserved quantities of the KdV equation. Evolution under the KdV equation guarantees the field-

line independence of these quantities. Thirdly, we can estimate the maximum toroidal volume QS allows solely from the properties of the roots and independent of any particular geometry. The overlap of the third root with the second signals the breakdown of periodicity of B , as demonstrated numerically. Finally, the connection length can be much larger than the major radius, typically assumed in the literature. A longer connection length may have important implications for linear and nonlinear stability in devices with QS.

Our third approach is data-driven. Utilizing the vast amount of data on quasisymmetric equilibria generated in [36] and the QUASR database [37], and the state-of-the-art tool pySINDy, which uses sparse regression techniques to discover underlying models, we recover KdV and Gardner's equation. Thus, the Painlevé property that demands that $(\partial_\ell B)^2$ can be at most a quartic in B is verified accurately. This data-driven approach has the advantage that it can be applied to any configuration (including when quasi-symmetry is not relevant) to find low-dimensional ODE or PDE models underlying the data.

Given the well-known robust stability of soliton solutions [83], the spectral stability of the cnoidal waves [84], and the robustness of the single-valuedness criterion, which led to the Painlevé property, perhaps explain why any numerical optimizer trying to find good QS using the 2-term form or the triple product form will most likely find only cubic or quartic terms in $(\partial_\ell B)^2$.

ACKNOWLEDGMENTS

We conclude by thanking P. Helander, B. Khesin, J.W. Burby, M. Wheeler, J. Meiss, N. Duignan, V. Duarte, H. Weitzner, E. Rodriguez, F.P. Diaz and M. Landreman for helpful discussions and suggestions. This research was supported by a grant from the Simons Foundation/SFARI (560651, AB) and DoE Grant No. DE-AC02-09CH11466.

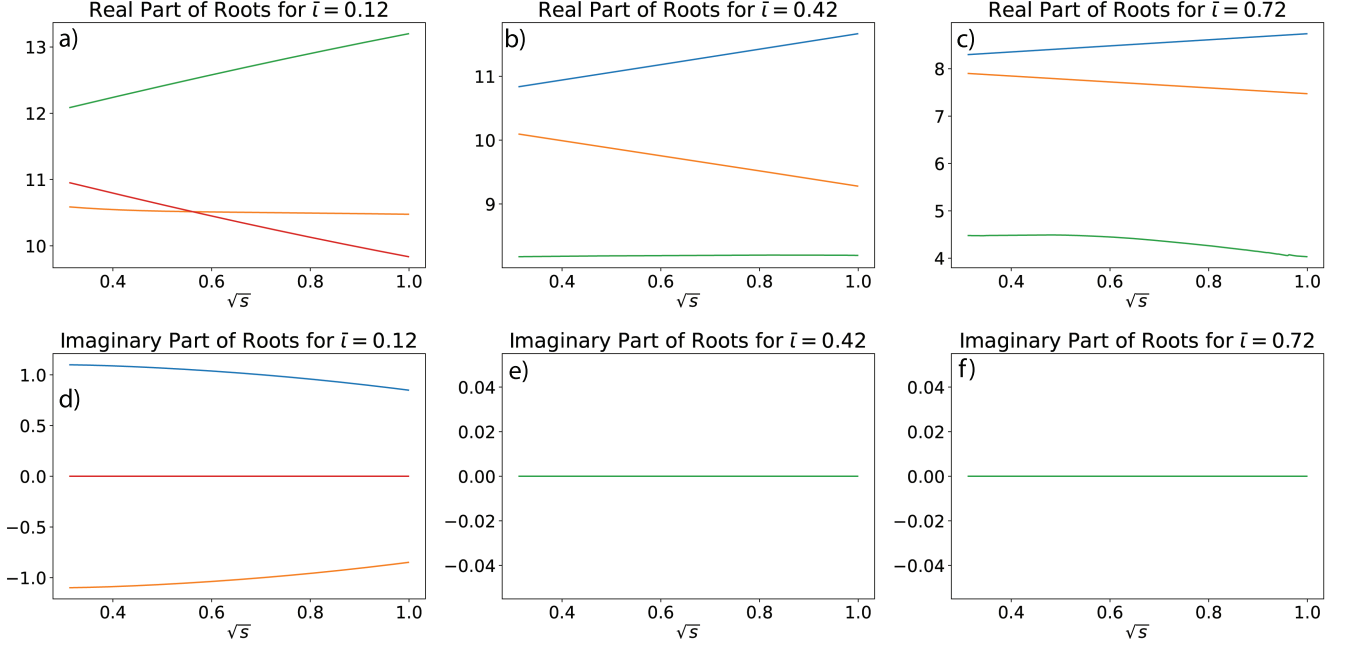


FIG. 19. $(\partial_t B)^2$ is fit to a polynomial of B across all flux surfaces – a cubic in all cases except c), which is fit to a quartic as per Fig. 14. Shown is the evolution of the roots.

Appendix A: The QS condition $\mathbf{u} \cdot \nabla B = 0$ in Clebsch variables

In the Clebsch coordinates (ψ, α, ℓ) with $\mathbf{B} \cdot \nabla \ell = B$, the operators $\mathbf{B} \cdot \nabla, \mathbf{u} \cdot \nabla$ take the form

$$\mathbf{B} \cdot \nabla = B \partial_\ell, \quad \mathbf{u} \cdot \nabla = \mathbf{u} \cdot \nabla \alpha \partial_\alpha + \mathbf{u} \cdot \nabla \ell \partial_\ell \quad (\text{A1})$$

It follows from the expression for \mathbf{u} given in (3) that $\mathbf{u} \cdot \nabla \alpha = -1$. Defining $H \equiv \mathbf{u} \cdot \nabla \ell$, we can express the QS condition $\mathbf{u} \cdot \nabla B = 0$ as

$$\mathbf{u} \cdot \nabla B = -\partial_\alpha B + H \partial_\ell B = 0. \quad (\text{A2})$$

We can use the fact that the commutator $[\mathbf{u} \cdot \nabla, \mathbf{B} \cdot \nabla] = 0$ and the QS condition (A2) to show that

$$\partial_\ell H = 0, \quad \text{i.e.,} \quad H = H(\psi, \alpha). \quad (\text{A3})$$

In axisymmetry, the expressions for the vectors \mathbf{B}, \mathbf{u} in standard cylindrical coordinates (R, ϕ, z) are given by

$$\mathbf{B} = F(\psi) \nabla \phi + \nabla \phi \times \nabla \psi, \quad \mathbf{u} = R^2 \nabla \phi, \quad (\text{A4})$$

where ι, ψ denotes the rotational transform and the poloidal flux. It is convenient to define a flux coordinate [48] (ψ, θ, ϕ) such that the Jacobian $1/\sqrt{g} = \nabla \psi \times \nabla \theta \cdot \nabla \phi = F/R^2$. In the flux coordinates, we have

$$\mathbf{B} = \nabla \psi \times \nabla \alpha, \quad \alpha = \iota^{-1} \theta - \phi, \quad (\text{A5a})$$

$$\mathbf{B} \cdot \nabla = \frac{1}{\sqrt{g}} (\partial_\phi + \iota \partial_\theta), \quad \mathbf{u} \cdot \nabla = \partial_\phi. \quad (\text{A5b})$$

It is easy to check that $\mathbf{B} \cdot \nabla, \mathbf{u} \cdot \nabla$ commute since $\partial_\phi \sqrt{g} = 0$ in axisymmetry.

Now, we go to the Clebsch coordinates (ψ, α, ℓ) to express H in terms of the flux coordinate system we just introduced. The quantity ℓ can be determined by the following ODE describing a field line

$$\frac{d\ell}{B} = \frac{d\phi}{\mathbf{B} \cdot \nabla \phi} = \frac{d\theta}{\mathbf{B} \cdot \nabla \theta}. \quad (\text{A6})$$

Utilizing $d\theta = \iota d\phi$, $\mathbf{B} \cdot \nabla \phi = 1/\sqrt{g}$ and integrating along the field line keeping ψ, α fixed, we get

$$\ell = \frac{1}{\iota} \int_{\psi, \alpha} B \sqrt{g} d\theta, \quad (\text{A7})$$

upto an overall function $h(\psi, \alpha)$, which can be set to zero by appropriately choosing the lower bound of the integral. Changing the coordinates from (ψ, θ, ϕ) to (ψ, α, θ) such that

$$\phi = \iota^{-1} \theta - \alpha, \quad \mathbf{B} \cdot \nabla = (\iota/\sqrt{g}) \partial_\theta, \quad \mathbf{u} \cdot \nabla = -\partial_\alpha, \quad (\text{A8})$$

we can calculate the quantities $\mathbf{B} \cdot \nabla \ell$ and $\mathbf{u} \cdot \nabla \ell$. It is easily checked that $\mathbf{B} \cdot \nabla \ell = B$ as it should be. On the other hand, $\mathbf{u} \cdot \nabla \ell$ and hence H vanishes since a perfectly axisymmetric B and \sqrt{g} depend only on ψ, θ .

A similar analysis can be carried out in standard Boozer coordinates $(\psi, \vartheta_B, \phi_B)$ [27] where

$$\mathbf{B} = \nabla \psi \times \nabla \vartheta_B + \iota_N \nabla \phi_B \times \nabla \psi, \quad (\text{A9a})$$

$$\mathbf{B} = (G + NI) \nabla \phi_B + I \nabla \vartheta_B + K \nabla \psi, \quad (\text{A9b})$$

$$1/\sqrt{g} = B^2/(G + \iota I), \quad \iota_N = \iota - N \quad (\text{A9c})$$

If B is quasisymmetric, $B = B(\psi, \vartheta_B)$ in the Boozer coordinate. Following the same steps as before, we obtain in $(\psi, \alpha, \vartheta_B)$ coordinates

$$\mathbf{B} \cdot \nabla = \frac{\iota_N}{\sqrt{g}} \partial_{\vartheta_B}, \quad \mathbf{u} \cdot \nabla = -\partial_\alpha, \quad (\text{A10a})$$

$$\ell = \frac{1}{\iota_N} \int_\alpha \sqrt{g} B d\vartheta_B. \quad (\text{A10b})$$

If QS is perfect, $\mathbf{u} \cdot \nabla \ell$ would perfectly vanish because the Jacobian of Boozer coordinates is a function of B and flux. However, for an approximately quasisymmetric system, the Jacobian depends on α . Consequently, the $\mathbf{u} \cdot \nabla \ell$ term does not vanish and can introduce a nonzero α dependent H .

Appendix B: Derivation of the KdV equation for vacuum quasisymmetric B in slab geometry

We shall now present a detailed derivation of the KdV equation in slab geometry. There are several steps in the calculation and we shall present them in the following subsections. First, we show the consistency of (24c) with the two-term form of QS. Second, we derive the relation between (ψ, α, ℓ) and the Cartesian coordinates. Third, we derive the expressions for H . Finally, we expand the GB and the KBC equations order by order.

1. Equivalence of (24c) and the two-term form of QS

We first point out the equivalence of (24c) to the two-term relation. Since the QS condition has not appeared directly in the form (24c) to the best of our knowledge, let us point out its relation to one of the standard forms of QS. To impose QS on the vacuum field, we can use the two-term form (4). We find that

$$\nabla \psi \times \nabla \left(\Phi + \frac{F(\psi)}{G_0} \alpha \right) \cdot \nabla B = 0 \quad (\text{B1})$$

Thus, for vacuum fields B satisfies a travelling-wave-like solution [47] in (Φ, α) of the form [47]

$$B = B(\Phi + \alpha F(\psi)/G_0, \psi) \quad (\text{B2})$$

Equivalently, $B = B(\vartheta, \psi)$ in Boozer coordinates.

On the other hand, eliminating H from (24c) using (13) we find that

$$\{\Phi + \alpha F(\psi)/G_0, B\}_{(\alpha, \ell)} = 0 \Leftrightarrow \{\vartheta_B, B\}_{(\alpha, \ell)} = 0 \quad (\text{B3})$$

where $\{, \}$ denotes the usual Poisson bracket with respect to (α, ℓ) . Therefore, (24c) is equivalent to the two-term form, while its ℓ derivative yields the relation (12). Equation (B3) also implies the equivalence of the TWs (7) and (16) in the Boozer and Clebsch coordinate systems.

2. Derivation of (31)

Next, we focus on the derivation of the (α, ℓ) derivatives. We shall use normalized variables for the derivations. We shall also use the fact that $\Phi_{,z} = O(\epsilon)$ from (30). Starting from the relation

$$\frac{d\ell}{B} = \frac{dx}{\Phi_{,x}} = \frac{dy}{\Phi_{,y}} = \frac{dz}{\Phi_{,z}} \quad (\text{B4})$$

we find that

$$\begin{aligned} \ell &= \int dx \sqrt{1 + \left(\frac{\Phi_{,y}}{\Phi_{,x}} \right)^2 + \left(\frac{\Phi_{,z}}{\Phi_{,x}} \right)^2} \\ \ell &\approx \int dx \left(1 + \frac{\epsilon^2}{2} (\varphi_{,y}^2 + \varphi_{,x}^2) \right) = x + O(\epsilon^2). \end{aligned} \quad (\text{B5})$$

To obtain ∂_ℓ we use the fact that in (ψ, α, ℓ) coordinates $\mathbf{B} \cdot \nabla = B \partial_\ell$. Thus,

$$\partial_\ell = \frac{1}{B} (\Phi_{,x} \partial_x + \Phi_{,y} \partial_y + \Phi_{,z} \partial_z) \quad (\text{B6})$$

A further simplification is possible due to the fact that

$$\begin{aligned} B &= |\nabla \Phi| = \sqrt{(1 + \epsilon \varphi_{,x})^2 + \epsilon^2 \varphi_{,y}^2 + \epsilon^2 \varphi_{,z}^2} \\ &\approx 1 + \epsilon \varphi_{,x} + \frac{\epsilon^2}{2} \varphi_{,y}^2. \end{aligned} \quad (\text{B7})$$

With the help of above, we find that

$$\partial_\ell = \frac{1}{1 + (\epsilon^2/2) \varphi_{,y}^2} (\partial_x + \epsilon \varphi_{,y} \partial_y + \varphi_{,z} \partial_z + O(\epsilon^2)) \quad (\text{B8})$$

Note that since $\varphi_{,z} = O(\epsilon)$, the $\epsilon^2 \varphi_{,z}^2$ term in (B7) is $O(\epsilon^4)$, whereas the $\varphi_{,z} \partial_z$ term in (B8) is $O(\epsilon)$. Hence we drop the former but not the latter. Also, note that in (B8) the $O(\epsilon^2)$ terms have y, z derivatives in them and when we calculate $\partial_\ell \Phi$, they do not contribute to $O(\epsilon^2)$ since $\Phi = x + O(\epsilon)$.

To derive ∂_α we shall make use of the fact that ℓ is essentially x up to $O(\epsilon^2)$. We also note that ∂_α is only needed on the uppermost surface, where $\psi = z - \epsilon \eta$. Thus,

$$\begin{aligned} \partial_\alpha &= \frac{1}{B} \nabla \ell \times \nabla \psi \cdot \nabla \\ &\approx \frac{\hat{\mathbf{x}} \times (\hat{\mathbf{z}} - \epsilon \eta_{,y} \sqrt{\epsilon} \hat{\mathbf{y}})}{1 + \epsilon \varphi_{,x}} \cdot \nabla = -\frac{(\partial_y + \epsilon \eta_{,y} \partial_z)}{1 + \epsilon \varphi_{,x}} \end{aligned} \quad (\text{B9})$$

3. Calculation of $H(\psi, \alpha)$

We shall calculate H from the derivatives of B using the expression for H (13), the expression for B (B7) and

the (α, ℓ) derivatives (31). Thus,

$$\begin{aligned} H &= \frac{\left(1 + \frac{\epsilon^2}{2}\varphi_{,y}^2\right) (\partial_y + \epsilon\eta_{,y}\partial_z) (\varphi_{,x} + \frac{\epsilon}{2}\varphi_{,y}^2)}{(1 + \epsilon\varphi_{,x}) (\partial_x + \epsilon\varphi_{,y}\partial_y + \varphi_{,z}\partial_z) (\varphi_{,x} + \frac{\epsilon}{2}\varphi_{,y}^2)} \\ &\approx \frac{(\varphi_{,xy} + \epsilon\varphi_{,y}\varphi_{,yy})}{(1 + \epsilon\varphi_{,x})(\varphi_{,xx} + 2\epsilon\varphi_{,y}\varphi_{,xy})} \quad (\text{B10}) \\ &= \frac{\varphi_{,xy}}{\varphi_{,xx}} + \epsilon \left(\frac{\varphi_{,y}\varphi_{,yy}}{\varphi_{,xx}} - \frac{\varphi_{,xy}}{\varphi_{,xx}} \left(\varphi_{,x} + 2\varphi_{,y}\frac{\varphi_{,xy}}{\varphi_{,xx}} \right) \right) \end{aligned}$$

Note that the $\varphi_{,z}$ terms do not enter because $\varphi_{,z} = O(\epsilon)$.

4. Generalized Bernoulli equation order by order

The GB equation (24c) implies

$$\frac{-\epsilon\varphi_{,y}}{1 + \epsilon\varphi_{,x}} + (H_0 + \epsilon H_1)(1 + \epsilon\varphi_{,x}) + q_0 + \epsilon\eta q_1 = 0 \quad (\text{B11})$$

Collecting powers of ϵ we get

$$H_0 + q_0 = 0, \quad (-\varphi_{,y} + H_1 + H_0\varphi_{,x} + \eta q_1) = 0. \quad (\text{B12})$$

The condition $H_0 + q_0 = 0$ together with the expression of H_0 from (B10) yields the TW solution $\varphi = \mathcal{A} = \mathcal{A}(\xi, Y)$ with $\xi = x - q_0 y, Y = \epsilon y$. Simplifying H_1 with the help of the TW solution leads to

$$H_1 = q_0 \mathcal{A}_{,\xi} (1 + q_0^2). \quad (\text{B13})$$

Substitution of (B13) into (B12) results in the following equation for η

$$-\eta \frac{q_1}{q_0} = (1 + q_0^2) \mathcal{A}_{,\xi}. \quad (\text{B14})$$

5. Kinematic boundary condition order by order

The KBC is obtained from the equation $\nabla\Phi \cdot \nabla\psi = 0$ with $\mathbf{B} = \nabla\Phi, \psi = z - \epsilon\eta$ and is given by

$$\varphi_{,z} = \epsilon\eta_{,x}(1 + \epsilon\varphi_{,x}) + \epsilon^2\varphi_{,y}\eta_{,y} \quad (\text{B15})$$

Owing to the fact that $\varphi_{,z} = O(\epsilon)$, we need to evaluate both sides to keep the $O(\epsilon^2)$ term in φ . We also need to keep both the scales y, Y in ∇_{\perp}^2 ,

$$\nabla_{\perp}^2 \rightarrow \partial_x^2 + (\partial_y + \epsilon\partial_Y)^2 = \nabla_{\perp}^2 + 2\epsilon\partial_Y\partial_y + \epsilon^2\partial_Y^2 \quad (\text{B16})$$

Finally, we note that (B15) has to be evaluated at $z = 1 + \epsilon\eta$.

Starting with

$$\varphi = \mathcal{A} - \epsilon \frac{z^2}{2!} \nabla_{\perp}^2 \mathcal{A} + \epsilon^2 \frac{z^4}{4!} \nabla_{\perp}^4 \mathcal{A}, \quad (\text{B17})$$

we find that the left side of the equation (B15) to be

$$\varphi_{,z} = \epsilon \left(-(1 + \epsilon\eta) \nabla_{\perp}^2 \mathcal{A} + \frac{\epsilon}{6} \nabla_{\perp}^4 \mathcal{A} \right) \quad (\text{B18})$$

Similarly, the right side of (B15) correct to $O(\epsilon^2)$ is

$$\epsilon (\eta_{,x} + \epsilon (\eta_{,x} \mathcal{A}_{,\xi} - q_0 \mathcal{A}_{,\xi} \eta_{,y})) \quad (\text{B19})$$

Equating both sides of (B15) we obtain

$$O(1): \quad (\eta_{,x} + \nabla_{\perp}^2 \mathcal{A}) = 0 \quad (\text{B20})$$

$$O(\epsilon): \quad 2q_0 \mathcal{A}_{,Y\xi} = \eta \nabla_{\perp}^2 \mathcal{A} + (\eta_{,\xi} - q_0 \eta_{,y}) \mathcal{A}_{,\xi} - \frac{1}{6} \nabla_{\perp}^4 \mathcal{A}$$

The TW frame and the TW form of \mathcal{A} leads to the following simplifications

$$\partial_x = \partial_{\xi}, \quad \partial_y = -q_0 \partial_{\xi} + \epsilon \partial_Y, \quad \nabla_{\perp}^2 \mathcal{A} = (1 + q_0^2) \mathcal{A}_{,\xi\xi} \quad (\text{B21})$$

Thus, (B20) yields

$$\eta = -(1 + q_0^2) \mathcal{A}_{,\xi}, \quad (\text{B22})$$

and

$$\frac{2q_0}{(1 + q_0^2)^2} \mathcal{A}_{,Y\xi} - \partial_{\xi} \left(\mathcal{A}_{,\xi} \frac{\eta}{1 + q_0^2} \right) + \frac{1}{6} \partial_{\xi}^4 \mathcal{A} = 0 \quad (\text{B23})$$

Substituting (B22) in (B23) we get

$$\frac{2q_0}{(1 + q_0^2)^2} \mathcal{A}_{,Y\xi} + 2\mathcal{A}_{,\xi} \mathcal{A}_{,\xi\xi} + \frac{1}{6} \partial_{\xi}^4 \mathcal{A} = 0 \quad (\text{B24})$$

Using $\tilde{B} = \mathcal{A}_{,\xi}$ we get the KdV equation for \tilde{B} given in (40).

For the subsidiary expansion in $C^{(1)}$ given in (45), (B23) takes the form

$$\frac{2q_0}{(1 + q_0^2)^2} \tilde{B}_{,Y} + \left(2\tilde{B} - 3C^{(1)}(1 + q_0^2) \tilde{B}^2 \right) \tilde{B}_{,\xi} + \frac{1}{6} \partial_{\xi}^3 \tilde{B} = 0. \quad (\text{B25})$$

Appendix C: Derivation of the KdV equation for vacuum quasisymmetric B in general geometry

We shall first assume complete orthogonality of the $(\Phi_s, \psi_s, \alpha_s)$ coordinates to simplify the calculations in C1. Then in C2 we drop the orthogonality requirement.

1. Orthogonal Boozer Coordinates

Proceeding under the orthogonality assumption and the other assumptions of Section III B, we now define

$$\begin{aligned} x &= \int \frac{d\Phi_s}{B_s}, \quad y = - \int \frac{d\alpha_s}{|\nabla\alpha_s|}, \quad z = \int \frac{d\psi_s}{|\nabla\psi_s|}, \quad (\text{C1}) \\ \hat{\mathbf{t}} &= \frac{\mathbf{B}_s}{B_s}, \quad \hat{\mathbf{y}} = - \frac{\nabla\alpha_s}{|\nabla\alpha_s|}, \quad \hat{\mathbf{z}} = \frac{\nabla\psi_s}{|\nabla\psi_s|}. \end{aligned}$$

The lower bounds of the integrals in (C1) are arbitrary. For the case of x , this freedom is analogous to the arbitrariness in choosing the origin of $\ell = 0$, which also leads to an arbitrariness in the definition of H as discussed in Section II.

We shall use the same normalization as in the slab case (27). In the (Φ_s, y, z) coordinates,

$$\nabla = \hat{z} \frac{1}{\sqrt{\epsilon}} \partial_z + \hat{y} \partial_y + \hat{t} B_s \partial_{\Phi_s} \quad (\text{C2})$$

Applying the gradient to Φ given in (48), we obtain

$$\begin{aligned} \mathbf{B} &= B_{\parallel} \hat{t} + \epsilon \hat{y} \varphi_{,y} + \sqrt{\epsilon} \varphi_{,z} \hat{z}, & B_{\parallel} &= B_s (1 + \epsilon \varphi_{,\Phi_s}) \\ \mathbf{B} \cdot \nabla &= B_{\parallel} B_s \partial_{\Phi_s} + \epsilon \varphi_{,y} \partial_y + \varphi_{,z} \partial_z \end{aligned} \quad (\text{C3})$$

The QS problem can now be formulated exactly as in (24). The system corresponding to (29) with the choice $z = 0$ on the innermost layer of the outer region, and $z = 1 + \epsilon \eta$ on the free-surface $\psi = \psi_s - \epsilon \eta$, reads

$$(B_s^2 \partial_{\Phi_s}^2 + \partial_y^2 + \epsilon^{-1} \partial_z^2) \varphi = 0 \quad (0 \leq z \leq 1 + \epsilon \eta) \quad (\text{C4a})$$

$$\partial_z \varphi = 0 \quad (z = 0) \quad (\text{C4b})$$

$$\partial_{\alpha}|_{\ell} \Phi + H \partial_{\ell} \Phi + q = 0 \quad (z = 1 + \epsilon \eta) \quad (\text{C4c})$$

$$|\nabla \psi_s|_{\varphi,z} = \epsilon B_s \eta_{,\Phi_s} B_{\parallel} + \epsilon^2 \varphi_{,y} \eta_{,y} \quad (z = 1 + \epsilon \eta). \quad (\text{C4d})$$

Note that the QS condition (C4c) is the relation $\mathbf{u} \cdot \nabla \Phi = F(\psi)/G_0$ written in terms of (ψ, α, ℓ) coordinates as before.

The expressions for the analog of (31) and (32) are

$$\begin{aligned} \ell &= x + O(\epsilon^2), & \partial_{\ell} &= \partial_{\ell_s} + \frac{\varphi_{,x}}{B_{\parallel}} \partial_x + \epsilon \frac{\varphi_{,y}}{B_{\parallel}} \partial_y + O(\epsilon^2) \\ \partial_{\alpha} &= \frac{\partial_{\alpha_s} + \epsilon \eta_{,\alpha_s} \partial_{\psi_s}}{B_{\parallel}/B_s}, & H_0 &= -\frac{\partial_{\alpha_s} B_s}{\partial_{\ell_s} B_s} \\ \frac{H_1}{H_0} &= -\varphi_{,\Phi_s} - \frac{\varphi_y}{B_{\parallel}} \frac{\partial_y B_s}{\partial_x B_s} + \frac{B_s}{H_0 \partial_x B_s} (\partial_{\alpha_s} + H_0 \partial_x) \varphi_{,\Phi_s} \end{aligned} \quad (\text{C5})$$

The derivation of the above quantities are parallel to the slab geometry. Therefore, we omit the details and focus on the differences due to the geometries. The small differences between the two geometries follow from the fact that the lowest order B is a constant in the slab geometry, which is not the case in general geometry. As a result, the expressions for H are different. In particular, in the slab geometry we had to keep corrections up to $O(\epsilon^2)$ since derivatives of B vanished to lowest order. Here, $O(\epsilon)$ terms suffice, making the analysis easier.

Proceeding with the solutions of (C4), we find that φ has the same form as the slab geometry solution (30). Next, evaluating the QS condition (C4c) to lowest order we find

$$\partial_{\alpha_s} \Phi_s + H_0 \partial_x \Phi_s + q_0 = 0, \quad \partial_{\alpha_s} B_s + H_0 \partial_x B_s = 0, \quad (\text{C6})$$

which leads to the following solutions for B_s, Φ_s in

(ℓ_s, α_s) variables

$$\begin{aligned} B_s &= B_s(\xi), & \xi &= x - \int H_0 d\alpha_s \\ \Phi_s &= -q_0 \alpha_s + \mathcal{B}_s^{-1}(\xi). \end{aligned} \quad (\text{C7})$$

Equation (C7) captures the essence of QS. It shows that B to lowest order is a TW, in both (α_s, x) and (Φ_s, α_s) variables, i.e.,

$$B_s = B_s(\xi) = \mathcal{B}_s(\Phi_s + q_0 \alpha_s). \quad (\text{C8})$$

Since the TW property of B is true nonperturbatively as well, it implies that B_{\parallel} and therefore $\varphi_{,\Phi_s}$ must also be TWs of the form (C8). Integrating over Φ_s we find that φ must itself be a TW. Thus, the slab geometry solution (B17) then reads

$$\begin{aligned} \varphi &= \mathcal{A}(\xi, \epsilon Y) - \frac{\epsilon z^2}{2} (\partial_x^2 + \partial_y^2) \mathcal{A} + O(\epsilon^2) \\ &= \mathcal{A} - \frac{\epsilon z^2}{2} (1 + H_0^2 |\nabla \alpha_s|^2) \mathcal{A}_{,xx} + O(\epsilon^2). \end{aligned} \quad (\text{C9})$$

Here, $Y = \epsilon y$ is a longer length scale in y and we have used

$$\partial_y = |\nabla \alpha_s| \partial_{\alpha_s}, \quad \partial_{\alpha_s} \xi = -H_0 \partial_x \xi. \quad (\text{C10})$$

The TW property of B_s, φ helps simplify the expression of H_1 to

$$H_1 = -\frac{H_0}{B_s} (1 + |\nabla \alpha_s|^2 H_0^2) \varphi_{,\xi} \quad (\text{C11})$$

analogous to (B13) from the slab case. Note that unlike the slab limit, H_0 is not necessarily $-q_0$. Finally, the expression for η (analogous to (B14)) obtained from the $O(\epsilon)$ QS condition (C4c), is given by

$$-\frac{q_1}{q_0} \eta_1 = (1 + H_0^2 |\nabla \alpha_s|^2) \frac{\varphi_{,\xi}}{B_s} \quad (\text{C12})$$

Next, we turn to the KBC (C4d). We can rewrite (C4d) as

$$|\nabla \psi_s|_{\varphi,z} = \epsilon \eta_{,x} (B_s 1 + \epsilon \varphi_{,x}) + \epsilon^2 \varphi_{,y} \eta_{,y} \quad (z = 1 + \epsilon \eta). \quad (\text{C13})$$

To $O(\epsilon)$ (C13) leads to

$$\epsilon \eta_{,x} = \frac{|\nabla \psi_s|}{B_s} \varphi_{,z} \quad (\text{C14})$$

Substituting the expression for φ (C9) in (C14) we get

$$-\eta = \frac{|\nabla \psi_s|}{B_s} (1 + |\nabla \alpha_s|^2 H_0^2) \mathcal{A}_{\xi} \quad (\text{C15})$$

Thus, the compatibility between QS (C12) and force-balance (C15) yields a specific value of q_1/q_0 (analogous to (38))

$$q_1 = q_0 |\nabla \psi_s|. \quad (\text{C16})$$

From $O(\epsilon^2)$, proceeding just as in the slab geometry case, we obtain the KdV equation for A_ξ

$$\begin{aligned} C_1 \mathcal{A}_{,Y\xi} + C_2 \mathcal{A}_\xi \mathcal{A}_{,\xi\xi} + \frac{1}{6} C_3 \partial_\xi^4 \mathcal{A} &= 0 \\ C_1 &= \frac{2\hat{q}}{C_3}, \quad C_2 = 1 + \frac{|\nabla\psi_s|}{B_s} C_3, \\ C_3 &= (1 + \hat{q}^2), \quad \hat{q} = H_0 |\nabla\alpha_s| \end{aligned} \quad (\text{C17})$$

By assumption B_s varies only weakly. Therefore, by construction $B \approx B_s + \epsilon \mathcal{A}_\xi$ also satisfies the KdV equation. The weakly varying assumption on B_s can be relaxed but we leave that details to future work. In fact, the NAE description of B_s is indeed consistent with the KdV equation, as shown in Section V. Finally, the modification for small ι can be done using a subsidiary expansion of (C12). We omit the details because it parallels the slab geometry description.

2. Non-orthogonal Boozer Coordinates

We shall now consider generic Boozer coordinates that are non-orthogonal. We choose the orthogonal triad $(\hat{\mathbf{x}}, \hat{\mathbf{y}}, \hat{\mathbf{z}})$ such that $\hat{\mathbf{x}}$ is aligned with the unit vector $\hat{\mathbf{t}}$ along the magnetic field \mathbf{B}_s . Let λ be the angle that characterize the non-orthogonality of the system and is defined by

$$\sin 2\lambda = -\frac{\nabla\psi_s \cdot \nabla\alpha_s}{|\nabla\psi_s| |\nabla\alpha_s|}. \quad (\text{C18})$$

In terms of λ we have

$$\begin{aligned} \frac{\nabla\psi_s}{|\nabla\psi_s|} &= \cos \lambda \hat{\mathbf{z}} + \sin \lambda \hat{\mathbf{y}} \\ \frac{\nabla\alpha_s}{|\nabla\alpha_s|} &= -\cos \lambda \hat{\mathbf{y}} - \sin \lambda \hat{\mathbf{z}} \end{aligned} \quad (\text{C19})$$

The magnetic field, given by $\mathbf{B}_s = \nabla\psi_s \times \nabla\alpha_s$, yields

$$\mathbf{B}_s = B_s \hat{\mathbf{z}}, \quad B_s = |\nabla\psi_s| |\nabla\alpha_s| \cos 2\lambda \quad (\text{C20})$$

Expressions (C19) and (C20) determine the the covariant basis vectors

$$\mathbf{e}^1 = \nabla\psi_s, \quad \mathbf{e}^2 = \nabla\alpha_s, \quad \mathbf{e}^3 = B_s \hat{\mathbf{z}} \quad (\text{C21})$$

The Jacobian of the $(\psi_s, \alpha_s, \Phi_s)$ system is $J^{-1} = B_s^2$. The contravariant vectors [48] are easily seen to be

$$\begin{aligned} \mathbf{e}_1 &= \frac{|\nabla\alpha_s|}{B_s} (\hat{\mathbf{z}} \cos \lambda - \hat{\mathbf{y}} \sin \lambda), \quad \mathbf{e}_3 = \frac{\hat{\mathbf{z}}}{B_s} \\ \mathbf{e}_2 &= \frac{|\nabla\psi_s|}{B_s} (-\hat{\mathbf{y}} \cos \lambda + \hat{\mathbf{z}} \sin \lambda) \end{aligned} \quad (\text{C22})$$

The basis vectors are related to each other through

$$\begin{aligned} \mathbf{e}^1 &= \frac{B_s |\nabla\psi_s|}{\cos 2\lambda} \left(\frac{1}{|\nabla\psi_s|} \mathbf{e}_1 - \sin 2\lambda \frac{\mathbf{e}_2}{|\nabla\alpha_s|} \right), \quad \mathbf{e}^3 = B_s^2 \mathbf{e}_3 \\ \mathbf{e}^2 &= \frac{B_s |\nabla\psi_s|}{\cos 2\lambda} \left(\frac{1}{|\nabla\psi_s|} \mathbf{e}_2 - \sin 2\lambda \frac{\mathbf{e}_1}{|\nabla\alpha_s|} \right) \end{aligned} \quad (\text{C23})$$

Using the basis vectors and the relationship between them (C23) we find

$$\begin{aligned} \nabla\varphi &= \mathbf{B}_s \varphi_{,\Phi_s} \\ &+ |\nabla\psi_s| \mathbf{e}_1 \left(\frac{1}{\sqrt{\epsilon}} \varphi_{,\psi_s} |\nabla\psi_s| - \varphi_{,\alpha_s} |\nabla\alpha_s| \sin 2\lambda \right) \\ &+ |\nabla\alpha_s| \mathbf{e}_2 \left(-\sin 2\lambda \frac{1}{\sqrt{\epsilon}} \varphi_{,\psi_s} |\nabla\psi_s| + \varphi_{,\alpha_s} |\nabla\alpha_s| \right). \end{aligned} \quad (\text{C24})$$

Using the same definitions of (x, y, z) as in (C1) we can show that the Laplacian is now given by

$$\nabla^2 \varphi = \frac{1}{\epsilon} \varphi_{,zz} + \varphi_{,yy} + 2 \sin 2\lambda \frac{1}{\sqrt{\epsilon}} \varphi_{,yz} + B_s^2 \partial_{\Phi_s}^2 \varphi. \quad (\text{C25})$$

The solution of (C25) can be seen to be of the form

$$\begin{aligned} \varphi &= \mathcal{A}(x, y) + \epsilon \varphi_1 + \epsilon^{3/2} \varphi_{3h} + \epsilon^2 \varphi_2 \\ -\varphi_1 &= \frac{z^2}{2!} (\partial_x^2 + \partial_y^2) \mathcal{A}, \quad \varphi_2 = \frac{z^4}{4!} (\partial_x^2 + \partial_y^2)^2 \mathcal{A} \\ -\partial_z^2 \varphi_{3h} &= 2 \sin 2\lambda \partial_{yz}^2 \varphi_1 \end{aligned} \quad (\text{C26})$$

Thus, we see that the effect of the non-orthogonality is mainly to produce an off-diagonal term in the Laplacian (C25), which leads to a fractional power $O(\epsilon^{3/2})$ term φ_{3h} . The effect of non-orthogonality on φ is seen to be small compared to the $O(\epsilon)$ correction. Moreover, because of the odd fractional power, φ_{3h} does not change φ_1, φ_2 , which enters into the QS condition and the KdV equation. Thus, φ_{3h} is a correction term that is completely determined by \mathcal{A} and does not couple back to the quantities of interest.

Next we calculate $\mathbf{B} \cdot \nabla$ and the (α, ℓ) derivatives. From (C24) it follows that

$$\frac{dx}{B_{||}} = \frac{dz}{\varphi_{,z} + \sqrt{\epsilon} \varphi_{,y} \sin 2\lambda} = \frac{dy}{\epsilon \varphi_{,y} + \sqrt{\epsilon} \varphi_{,z} \sin 2\lambda} \quad (\text{C27})$$

leading to

$$\ell = x + \epsilon \ell_1 + O(\epsilon^{3/2}) \quad \ell_1 \equiv \int \frac{dx}{B_s^2} \frac{\sin^2 2\lambda}{2} \varphi_{,y}^2 \quad (\text{C28})$$

Due to the $O(\epsilon)$ correction in ℓ as compared to $O(\epsilon^2)$ in the orthogonal case (C5), ∂_α has a correction of $O(\epsilon)$ driven by the non-orthogonality

$$\partial_\alpha = \frac{B_s}{B_{||}} (\partial_{\alpha_s} + \epsilon \eta_{,\alpha_s} \partial_\psi + \epsilon \{, \ell_1 \}_{(\alpha_s, x)}) + O(\epsilon^{3/2}) \quad (\text{C29})$$

In the calculation of the QS condition (34) we need ∂_α to first order. Therefore, the non-orthogonal correction is relevant. However, the correction term is in the form of a Poisson bracket. Fortunately, due to the TW form of φ, B , this term cancels out.

Therefore, we find that although there are differences in the orthogonal and the non-orthogonal Boozer coordinates approach, the conclusions drawn from using the orthogonal approach are not changed within the required precision.

Appendix D: Derivation of $\mathcal{D}(\psi)$ in equation (12)

We present here the derivation of the function $\mathcal{D}(\psi)$, which appears in

$$\left(\frac{\partial B}{\partial \ell}\right)^2 = \mathcal{D}(\psi)(B_M - B)(B - B_m)(B - B_X), \quad (12)$$

in terms of the roots $B_M(\psi), B_m(\psi), B_X(\psi), \iota(\psi)$, the rotational transform, and the quasihelicity N [11, 27].

For the derivation, we shall utilize the following facts. Firstly, B is periodic with period $L(\psi)$. Thus, $B(\ell) = B(\ell + L(\psi))$. Secondly, the average $\oint B d\ell$ is a flux function. To show this, we use Boozer coordinates (ψ, ϑ, ϕ) [27], where the Jacobian is given by

$$\mathbf{B} \cdot \nabla \vartheta = \iota_N \frac{B^2}{G(\psi) + \iota(\psi)I(\psi)}, \quad \iota_N = \iota(\psi) - N. \quad (D1)$$

Note that $G(\psi), I(\psi)$ are flux functions related to the poloidal and toroidal currents. [11] Since $\mathbf{B} \cdot \nabla = B \partial_\ell$ in (ψ, α, ℓ) , (D1) takes the form

$$\frac{\partial \vartheta}{\partial \ell} = \iota_N \frac{B}{G + \iota I}. \quad (D2)$$

Integrating (D2) with respect to ℓ from 0 to L and noting that the net change in the Boozer angle ϑ is 2π , we get

$$\int_0^L B d\ell = 2\pi \frac{G + \iota I}{\iota_N}. \quad (D3)$$

Finally, we shall need some basic identities satisfied by elliptic functions (see Appendix A of reference [28]). In particular, we shall use

$$\begin{aligned} \text{dn}(z, m) &= \text{dn}(z + 2K(m), m) \\ \text{dn}^2(z, m) &= 1 - m + m \text{cn}^2(z, m) \\ \int_0^{K(m)} \text{dn}^2(u, m) du &= E(m), \end{aligned} \quad (D4)$$

where $\text{dn}(z, m), \text{cn}(z, m)$ are standard Jacobi elliptic functions, and $K(m), E(m)$ are the complete elliptic integrals of the first and second kind.[30]

We are now in a position to derive an expression for $\mathcal{D}(\psi)$. To simplify the derivation, we shall work in the frame of reference where $\partial_\alpha B = 0$ (see discussion under (3)). In this frame, the solution to (12) is

$$\begin{aligned} B &= B_X + (B_M - B_X) \text{dn}^2 \left(\sqrt{\frac{B_M - B_X}{2}} \sqrt{\frac{\mathcal{D}}{2}} \ell, m \right), \\ m &= \frac{B_M - B_m}{B_M - B_X}, \quad 0 \leq m \leq 1, \end{aligned} \quad (D5)$$

which follows from (13),(15) and (D4).

From the periodicity of B and the Jacobi elliptic function dn (D4), it follows that

$$\sqrt{\mathcal{D}} L(\psi) = \frac{4K(m)}{\sqrt{B_M - B_X}}. \quad (D6)$$

Moreover, integrating (D5) over ℓ we obtain

$$\int_0^L B d\ell = L \left(B_X + (B_M - B_X) \frac{E(m)}{K(m)} \right) \quad (D7)$$

Combining together the two different expressions of the $\oint B d\ell$ given by (D3) and (D7), and using the relation between \mathcal{D} and L from (D6), we finally obtain

$$\sqrt{\mathcal{D}} = \frac{\iota_N}{G + \iota I} \frac{K(m)}{\pi/2} \frac{\left(B_X + (B_M - B_X) \frac{E(m)}{K(m)} \right)}{\sqrt{B_M - B_X}} \quad (D8)$$

Appendix E: Additional configurations that satisfy the integrated KdV equation (12)

Here, we present figures similar to Figs. 1 and 3 in the main text, using data from different stellarator devices.

The precise QA configuration with larger negative shear in Fig. 21 was obtained by a series of optimizations starting from the precise QA.[4] Specifically, we start from the same objective function used to optimize the precise QA, and the precise QA configuration itself. The mean shear \hat{s} was extracted from the precise QA configuration, and a new least-squares term $(\hat{s} - \hat{s}_*)^2$ was added to the objective function, where the target value for mean shear \hat{s}_* is taken to be slightly different from the extracted value. This new objective is then optimized locally, using the precise QA as the initial state. This ensures that the additional least-squares term is almost zero, so the precise QA is approximately an optimum to the modified objective function. Hence, the new local optimum can be expected to be close to the initial configuration. This process is then repeated starting from the slightly modified optimum, each step generating a similar equilibrium with a slightly different mean shear. Mean shear is here defined as $b/\bar{\iota}$, where b is the result of fitting a first-order polynomial $a + bs$ to the iota profile, where s is the normalized toroidal flux; $\bar{\iota}$ is the rotational transform averaged over all radii. The mean shear in the original precise QA is about -0.018 , and we incremented the target negative shear in steps of 0.005 .

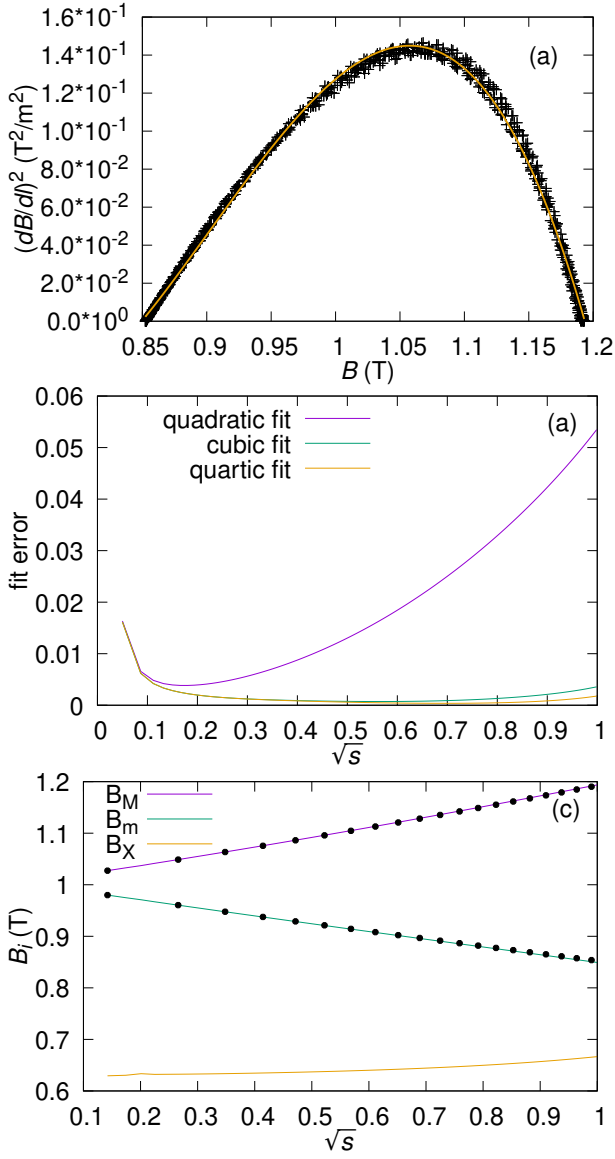


FIG. 20. The value of $(dB/d\ell)^2$ on the outermost flux surface in the precise QH [4] as a function of B , alongside a cubic polynomial fit (a), and the errors of quadratic, cubic, and quartic fits on each flux surface (b). Panel (c) shows the behavior of the roots in the precise QH.

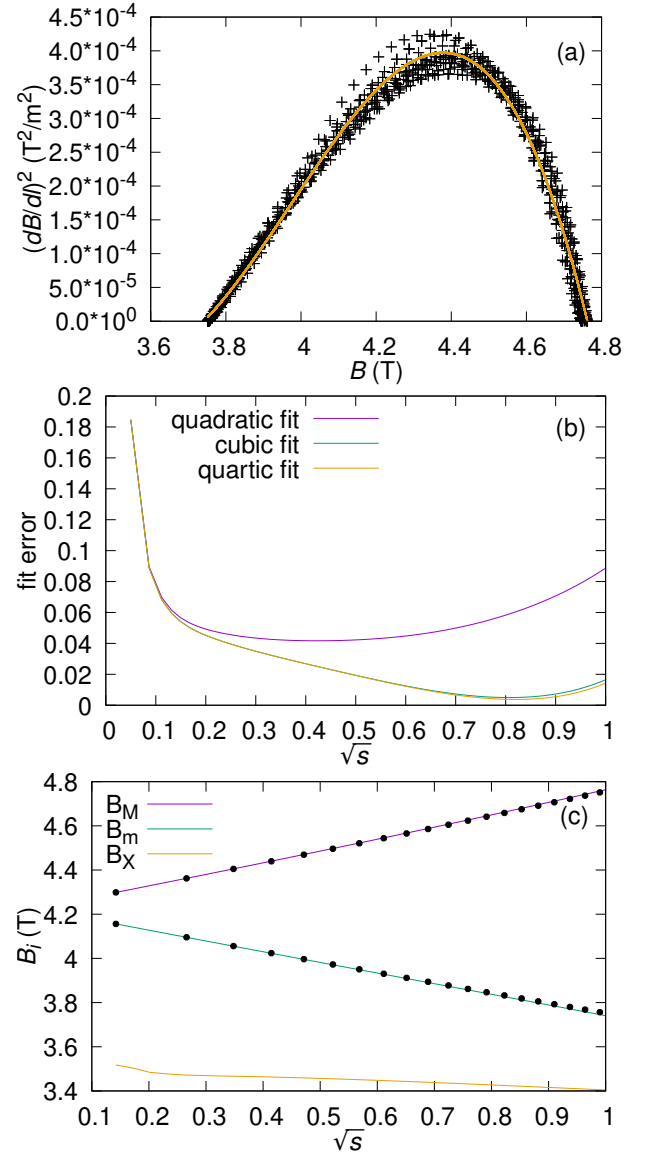


FIG. 21. The value of $(dB/d\ell)^2$ on the outermost flux surface in a precise QA version with average shear -0.08 as a function of B , alongside a cubic polynomial fit (a), and the errors of quadratic, cubic, and quartic fits on each flux surface (b). Panel (c) shows the behavior of the roots in this version of the precise QA.

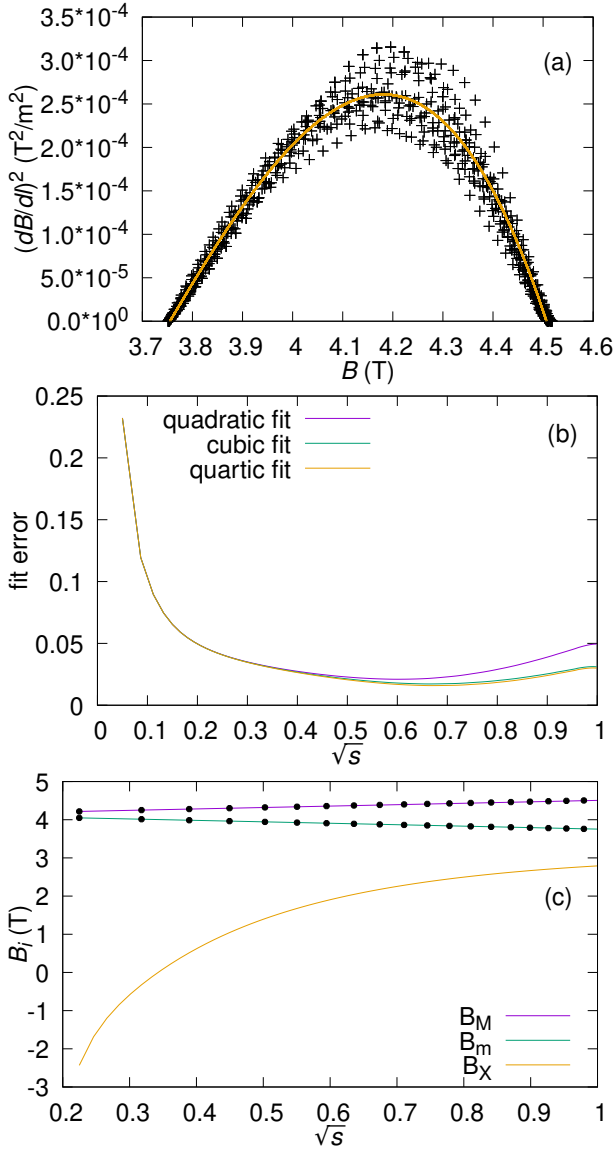


FIG. 22. The value of $(dB/dl)^2$ on the outermost flux surface in a precise QA version with average shear 0.04 as a function of B , alongside a cubic polynomial fit (a), and the errors of quadratic, cubic, and quartic fits on each flux surface (b). Panel (c) shows the behavior of the roots in this version of the precise QA.

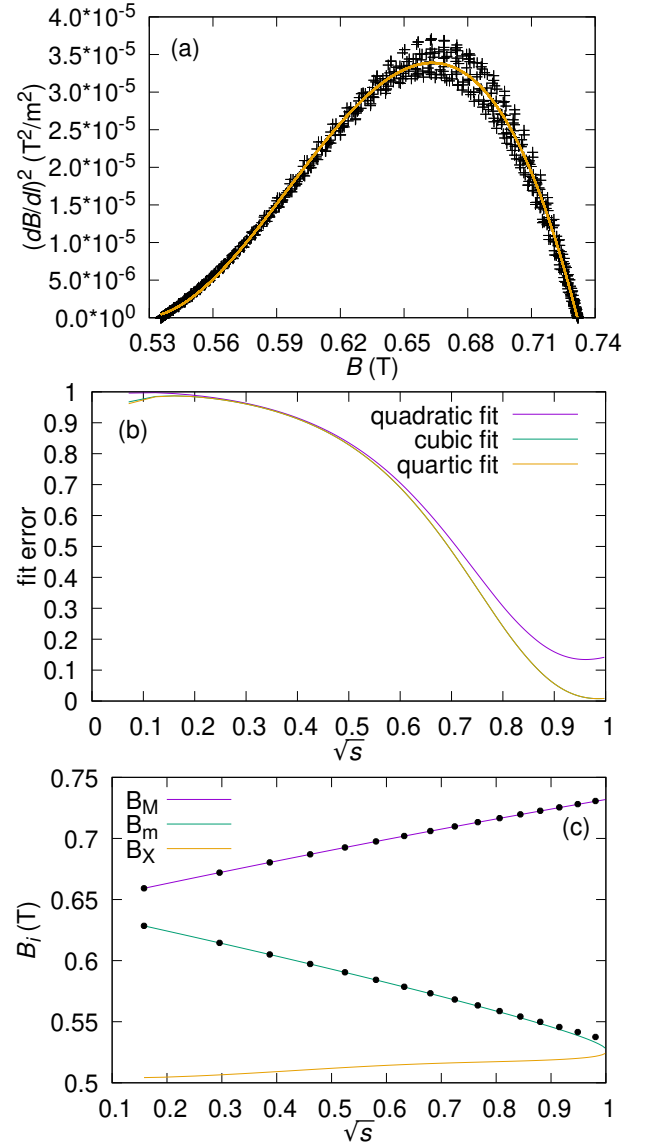


FIG. 23. The value of $(dB/dl)^2$ on the outermost flux surface in the QA equilibrium that was used in Fig. 2 in the main text as a function of B , alongside a cubic polynomial fit (a), and the errors of quadratic, cubic, and quartic fits on each flux surface (b). Panel (c) shows the behavior of the roots in this QA equilibrium.

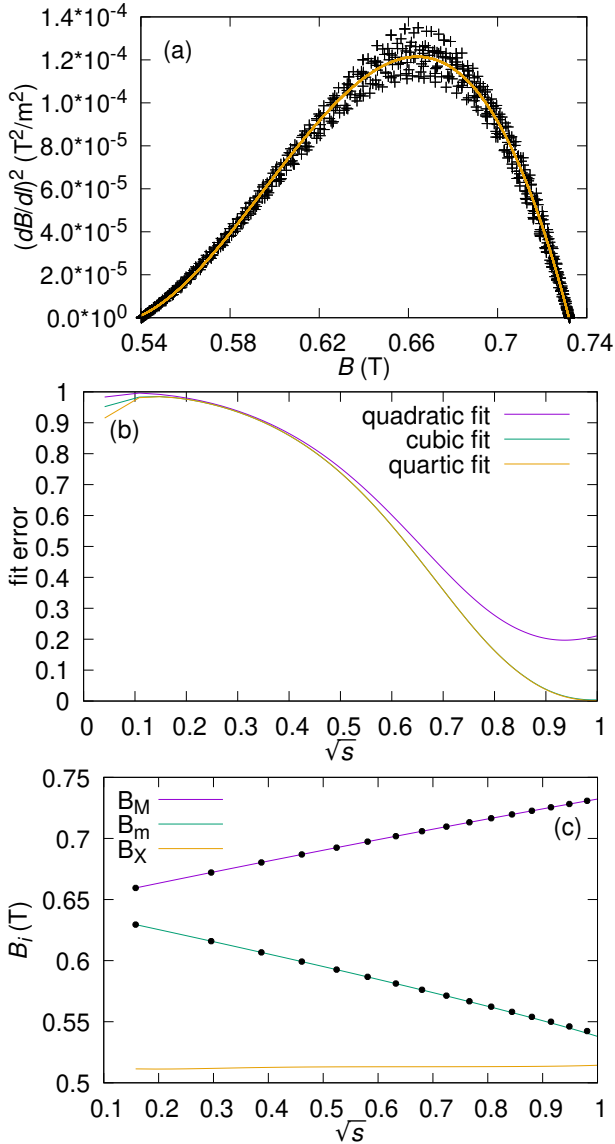


FIG. 24. The value of $(dB/dl)^2$ on the outermost flux surface in a QA equilibrium similar to that in Fig. 23 as a function of B , alongside a cubic polynomial fit (a), and the errors of quadratic, cubic, and quartic fits on each flux surface (b). Panel (c) shows the behavior of the roots in this QA equilibrium.

Figs. 23 and 24 show equilibria that were not derived from the precise QA/QH. Instead, they were only optimized for quasisymmetry on the outermost flux surface, with the quasisymmetry degrading as the axis is approached. For both cases, the ratio of symmetry-breaking modes to quasisymmetric modes near the axis is $\sim 10^{-3}$. While this may seem a small value, the resulting ripple creates enough noise in the $(dB/dl)^2$ vs. B plot to render it meaningless, and the error for all fits is ~ 1 in that region. The symmetry-breaking modes were filtered out when calculating the roots shown in panels (c). Note that the equilibrium shown in Fig. 23 is the same one used in Fig. 2 in the main text.

[1] P. Charalambous, S. Dubovsky, and M. M. Ivanov, Hidden symmetry of vanishing love numbers, *Physical Review Letters* **127**, 101101 (2021).
 [2] D. Lee, S. Bogner, B. A. Brown, S. Elhatisari, E. Epelbaum, H. Hergert, M. Hjorth-Jensen, H. Krebs, N. Li, B.-N. Lu, *et al.*, Hidden spin-isospin exchange symmetry, *Physical Review Letters* **127**, 062501 (2021).
 [3] Z. Liu and M. Tegmark, Machine learning hidden symmetries, *Physical Review Letters* **128**, 180201 (2022).
 [4] M. Landreman and E. Paul, Magnetic fields with precise quasisymmetry for plasma confinement, *Physical Review*

Letters **128**, 035001 (2022).
 [5] J. Moser, Hidden symmetries in dynamical systems, *American Scientist* **67**, 689 (1979).
 [6] P. G. Leach and K. Andriopoulos, The ermakov equation: a commentary, *Applicable Analysis and Discrete Mathematics*, 146 (2008).
 [7] V. Y. Ovsienko and B. A. Khesin, Korteweg-de vries superequation as an euler equation, *Functional Analysis and Its Applications* **21**, 329 (1987).
 [8] C. S. Gardner, J. M. Greene, M. D. Kruskal, and R. M. Miura, Method for solving the korteweg-devries equation,

- Physical review letters **19**, 1095 (1967).
- [9] S. Novikov, S. V. Manakov, L. P. Pitaevskii, and V. E. Zakharov, *Theory of solitons: the inverse scattering method* (Springer Science & Business Media, 1984).
- [10] A. H. Boozer, Transport and isomorphic equilibria, *The Physics of Fluids* **26**, 496 (1983).
- [11] P. Helander, Theory of plasma confinement in non-axisymmetric magnetic fields, *Reports on Progress in Physics* **77**, 087001 (2014).
- [12] E. Rodríguez, Quasisymmetry, Ph.D. thesis (2022).
- [13] N. Padhye and P. Morrison, *Relabeling symmetries in hydrodynamics and magnetohydrodynamics*, Tech. Rep. (Univ. of Texas, Austin, TX (United States). Institute for Fusion Studies, 1996).
- [14] G. Webb, *Magnetohydrodynamics and fluid dynamics: Action principles and conservation laws*, Vol. 946 (Springer, 2018).
- [15] H. Weitzner and W. Sengupta, Steady plasma flows in a periodic non-symmetric domain, *Journal of Plasma Physics* **87**, 905870603 (2021).
- [16] J. P. Freidberg, *Ideal MHD* (Cambridge University Press, 2014) p. 302.
- [17] D. A. Garren and A. H. Boozer, Magnetic field strength of toroidal plasma equilibria, *Physics of Fluids B: Plasma Physics* **3**, 2805 (1991).
- [18] D. A. Garren and A. H. Boozer, Existence of quasihelically symmetric stellarators, *Physics of Fluids B: Plasma Physics* **3**, 2822 (1991).
- [19] G. G. Plunk and P. Helander, Quasi-axisymmetric magnetic fields: weakly non-axisymmetric case in a vacuum, *Journal of Plasma Physics* **84**, 905840205 (2018).
- [20] M. Landreman and W. Sengupta, Constructing stellarators with quasisymmetry to high order, *Journal of Plasma Physics* **85**, 815850601 (2019).
- [21] P. Constantin, T. D. Drivas, and D. Ginsberg, On quasisymmetric plasma equilibria sustained by small force, *Journal of Plasma Physics* **87**, 905870111 (2021).
- [22] E. Rodríguez, P. Helander, and A. Bhattacharjee, Necessary and sufficient conditions for quasisymmetry, *Physics of Plasmas* **27**, 062501 (2020).
- [23] E. Rodríguez, W. Sengupta, and A. Bhattacharjee, Weakly quasisymmetric near-axis solutions to all orders, *Physics of Plasmas* **29**, 012507 (2022).
- [24] C. Mercier, Lectures in plasma physics: the magnetohydrodynamic approach to the problem of plasma confinement in closed magnetic configurations, Luxembourg Commission European Communities (1974).
- [25] L. S. Solov'ev and V. D. Shafranov, *Reviews of Plasma Physics 5* (Consultants Bureau, New York - London, 1970).
- [26] M. P. Bernardin, R. W. Moses, and J. A. Tataronis, Isodynamical (omnigenous) equilibrium in symmetrically confined plasma configurations, *The Physics of Fluids* **29**, 2605 (1986).
- [27] M. Landreman and W. Sengupta, Direct construction of optimized stellarator shapes. Part 1. Theory in cylindrical coordinates, *Journal of Plasma Physics* **84**, 905840616 (2018).
- [28] W. Schief, Nested toroidal flux surfaces in magnetohydrostatics. generation via soliton theory, *Journal of plasma physics* **69**, 465 (2003).
- [29] D. Palumbo, Some considerations on closed configurations of magnetohydrostatic equilibrium, *Nuovo Cimento B* **53**, 507 (1968).
- [30] A. M. Kamchatnov, *Nonlinear periodic waves and their modulations: an introductory course* (World Scientific, 2000).
- [31] R. M. Miura, C. S. Gardner, and M. D. Kruskal, Korteweg-de vries equation and generalizations. ii. existence of conservation laws and constants of motion, *Journal of Mathematical physics* **9**, 1204 (1968).
- [32] C. H. Su and C. S. Gardner, Korteweg—de vries equation and generalization. III. derivation of kdv and burgers equations, *J. Math. Phys* **10**, 536 (1969).
- [33] A. Kamchatnov, Y.-H. Kuo, T.-C. Lin, T.-L. Horng, S.-C. Gou, R. Clift, G. El, and R. H. Grimshaw, Undular bore theory for the gardner equation, *Physical Review E* **86**, 036605 (2012).
- [34] B. de Silva, K. Champion, M. Quade, J.-C. Loiseau, J. Kutz, and S. Brunton, Pysindy: A python package for the sparse identification of nonlinear dynamical systems from data, *Journal of Open Source Software* **5**, 2104 (2020).
- [35] A. A. Kaptanoglu, B. M. de Silva, U. Fasel, K. Kahe-man, A. J. Goldschmidt, J. Callahan, C. B. Delahunt, Z. G. Nicolaou, K. Champion, J.-C. Loiseau, J. N. Kutz, and S. L. Brunton, Pysindy: A comprehensive python package for robust sparse system identification, *Journal of Open Source Software* **7**, 3994 (2022).
- [36] S. Buller, M. Landreman, J. Kappel, and R. Gaur, A family of quasi-axisymmetric stellarators with varied rotational transform (2024), arXiv:2401.09021 [physics.plasm-ph].
- [37] A. Giuliani, Direct stellarator coil design using global optimization: application to a comprehensive exploration of quasi-axisymmetric devices (2023), arXiv:2310.19097 [physics.comp-ph].
- [38] I. Gजा and A. Bhattacharjee, Asymptotics of reflectionless potentials, *Physical review letters* **68**, 2413 (1992).
- [39] M. Berry and C. Howls, Fake airy functions and the asymptotics of reflectionlessness, *Journal of Physics A: Mathematical and General* **23**, L243 (1990).
- [40] J. W. Burby, N. Kallinikos, and R. S. MacKay, Some mathematics for quasi-symmetry, *Journal of Mathematical Physics* **61**, 093503 (2020).
- [41] N. Padhye and P. J. Morrison, Fluid element relabeling symmetry, *Physics letters A* **219**, 287 (1996).
- [42] R. Salmon, Hamilton's principle and ertel's theorem, in *AIP Conference Proceedings*, Vol. 88 (American Institute of Physics, 1982) pp. 127–135.
- [43] R. Salmon, Hamiltonian fluid mechanics, *Annual review of fluid mechanics* **20**, 225 (1988).
- [44] G. Webb and G. Zank, Fluid relabelling symmetries, lie point symmetries and the lagrangian map in magnetohydrodynamics and gas dynamics, *Journal of Physics A: Mathematical and Theoretical* **40**, 545 (2006).
- [45] E. Hameiri, The complete set of Casimir constants of the motion in magnetohydrodynamics, *Physics of plasmas* **11**, 3423 (2004).
- [46] A. H. Boozer, Guiding center drift equations, *The Physics of Fluids* **23**, 904 (1980), https://pubs.aip.org/aip/pfl/article-pdf/23/5/904/12463046/904_1_online.pdf.
- [47] W. Sengupta, E. J. Paul, H. Weitzner, and A. Bhattacharjee, Vacuum magnetic fields with exact quasisymmetry near a flux surface. part 1. solutions near an axisymmetric surface, *Journal of Plasma Physics* **87**, 905870205 (2021).

- [48] W. D. D’haeseleer, W. N. Hitchon, J. D. Callen, and J. L. Shohet, *Flux coordinates and magnetic field structure: a guide to a fundamental tool of plasma theory* (Springer Science & Business Media, 2012).
- [49] M. Barnes, F. I. Parra, and A. A. Schekochihin, Critically balanced ion temperature gradient turbulence in fusion plasmas, *Phys. Rev. Lett.* **107**, 115003 (2011).
- [50] M. Landreman and P. J. Catto, Omnigenity as generalized quasisymmetry, *Physics of Plasmas* **19** (2012).
- [51] J. R. Cary and S. G. Shasharina, Helical plasma confinement devices with good confinement properties, *Physical review letters* **78**, 674 (1997).
- [52] J. R. Cary and S. G. Shasharina, Omnigenity and quasi-helicity in helical plasma confinement systems, *Physics of Plasmas* **4**, 3323 (1997).
- [53] G. G. Plunk, M. Landreman, and P. Helander, Direct construction of optimized stellarator shapes. part 3. omnigenity near the magnetic axis, *Journal of Plasma Physics* **85**, 905850602 (2019).
- [54] M. Landreman, Mapping the space of quasisymmetric stellarators using optimized near-axis expansion, *Journal of Plasma Physics* **88**, 905880616 (2022).
- [55] T. Antonsen Jr, A. Ferreira, and J. Ramos, Perturbative study of the spectrum of large toroidal mode number ideal mhd instabilities, *Plasma Physics* **24**, 197 (1982).
- [56] B. Coppi, A. Ferreira, and J. J. Ramos, Self-healing of confined plasmas with finite pressure, *Physical Review Letters* **44**, 990 (1980).
- [57] R. D. Hazeltine and J. D. Meiss, Shear-alfvén dynamics of toroidally confined plasmas, *Physics Reports* **121**, 1 (1985).
- [58] M. J. Ablowitz, *Nonlinear dispersive waves: asymptotic analysis and solitons*, Vol. 47 (Cambridge University Press, 2011).
- [59] H. Weitzner and W. Sengupta, Exact non-symmetric closed line vacuum magnetic fields in a topological torus, *Physics of Plasmas* **27** (2020).
- [60] M. Kruskal, Asymptotology, in *Lectures presented at the Trieste Seminar on Plasma Physics* (1965) p. 373.
- [61] G. I. Burde and A. Sergeyev, Ordering of two small parameters in the shallow water wave problem, *Journal of Physics A: Mathematical and Theoretical* **46**, 075501 (2013).
- [62] R. M. Miura, The korteweg–devries equation: a survey of results, *SIAM review* **18**, 412 (1976).
- [63] W. Sengupta, N. Nikulsin, R. Gaur, and A. Bhattacharjee, Quasisymmetric high-beta 3d mhd equilibria near axisymmetry, arXiv preprint arXiv:2312.08572 (2023).
- [64] G. Plunk, Perturbing an axisymmetric magnetic equilibrium to obtain a quasi-axisymmetric stellarator, *Journal of Plasma Physics* **86**, 905860409 (2020).
- [65] N. Nikulsin, W. Sengupta, R. Jorge, and A. Bhattacharjee, An asymptotic grad-shafranov equation for quasisymmetric stellarators, arXiv preprint arXiv:2403.08022 (2024).
- [66] N. Sato, Existence of weakly quasisymmetric magnetic fields without rotational transform in asymmetric toroidal domains, *Scientific Reports* **12**, 11322 (2022).
- [67] R. Conte, *The Painlevé property: one century later* (Springer Science & Business Media, 2012).
- [68] D. Levi and P. Winternitz, *Painlevé transcendents: their asymptotics and physical applications*, Vol. 278 (Springer Science & Business Media, 2013).
- [69] E. Hille, *Ordinary differential equations in the complex domain* (Courier Corporation, 1997).
- [70] E. T. Whittaker and G. N. Watson, *A course of modern analysis: an introduction to the general theory of infinite processes and of analytic functions; with an account of the principal transcendental functions* (University press, 1920).
- [71] E. L. Ince, *Ordinary differential equations* (Courier Corporation, 1956).
- [72] M. D. Kruskal, N. Joshi, and R. Halburd, Analytic and asymptotic methods for nonlinear singularity analysis: a review and extensions of tests for the painlevé property, *Integrability of Nonlinear Systems: Proceedings of the CIMPA School Pondicherry University, India, 8–26 January 1996*, 171 (2007).
- [73] A. E. Eremenko, Meromorphic solutions of algebraic differential equations, *Russian Mathematical Surveys* **37**, 61 (1982).
- [74] E. A. Coddington, N. Levinson, and T. Teichmann, *Theory of ordinary differential equations* (1956).
- [75] M. J. Ablowitz, A. Ramani, and H. Segur, A connection between nonlinear evolution equations and ordinary differential equations of P-type. I, *Journal of Mathematical Physics* **21**, 715 (1980), https://pubs.aip.org/aip/jmp/article-pdf/21/4/715/19055961/715_1_online.pdf.
- [76] M. J. Ablowitz, A. Ramani, and H. Segur, A connection between nonlinear evolution equations and ordinary differential equations of P-type. II, *Journal of Mathematical Physics* **21**, 1006 (1980), https://pubs.aip.org/aip/jmp/article-pdf/21/5/1006/19093233/1006_1_online.pdf.
- [77] A. J. Cerfon and J. P. Freidberg, “one size fits all” analytic solutions to the grad-shafranov equation, *Physics of Plasmas* **17** (2010).
- [78] Y. V. Brezhnev, What does integrability of finite-gap or soliton potentials mean?, *Philosophical Transactions of the Royal Society A: Mathematical, Physical and Engineering Sciences* **366**, 923 (2008).
- [79] F. Wechsung, M. Landreman, A. Giuliani, A. Cerfon, and G. Stadler, Precise stellarator quasi-symmetry can be achieved with electromagnetic coils, *Proceedings of the National Academy of Sciences* **119**, e2202084119 (2022).
- [80] E. Rodríguez and A. Bhattacharjee, Islands and current singularities in quasisymmetric toroidal plasmas, *Physics of Plasmas* **28**, 092506 (2021).
- [81] S. L. Brunton, J. L. Proctor, and J. N. Kutz, Discovering governing equations from data by sparse identification of nonlinear dynamical systems, *Proceedings of the national academy of sciences* **113**, 3932 (2016).
- [82] L. Zhang and H. Schaeffer, On the convergence of the SINDy algorithm, *Multiscale Modeling & Simulation* **17**, 948 (2019).
- [83] T. Tao, Why are solitons stable?, *Bulletin of the American Mathematical Society* **46**, 1 (2009).
- [84] N. Bottman and B. Deconinck, Kdv cnoidal waves are spectrally stable, *Discrete and Continuous Dynamical Systems-Series A (DCDS-A)* **25**, 1163 (2009).